

Ecological communities from random Lotka-Volterra dynamics with nonlinear functional response

Laura Sidhom*

*Theoretical Physics, Department of Physics and Astronomy, School of Natural Sciences,
The University of Manchester, Manchester M13 9PL, United Kingdom*

Tobias Galla†

*Theoretical Physics, Department of Physics and Astronomy,
School of Natural Sciences, The University of Manchester,
Manchester M13 9PL, United Kingdom and
Instituto de Física Interdisciplinar y Sistemas Complejos, IFISC (CSIC-UIB),
Campus Universitat Illes Balears, E-07122 Palma de Mallorca, Spain*

(Dated: January 14, 2023)

We investigate the outcome of Lotka-Volterra dynamics of ecological communities with random interaction coefficients and non-linear functional response. We show in simulations that the saturation of Holling type-II response stabilises the dynamics. This is confirmed in an analytical generating-functional approach to Lotka-Volterra equations with piecewise linear saturating response. For such systems we are able to derive self-consistent relations governing the stable fixed-point phase, and to carry out a linear stability analysis to predict the onset of unstable behaviour. We investigate in detail the combined effects of the mean and variance of the random interaction coefficients, the cut-off parameter of the non-linear response, and a symmetry parameter. We find that stability and diversity increases with the introduction of functional response, where decreasing the functional response parameter has a similar effect to decreasing the symmetry parameter. We also find biomass and diversity to be less dependent on the symmetry of interactions with functional response, and co-operation to no longer have a detrimental effect on stability.

* laura.sidhom@postgrad.manchester.ac.uk

† tobias.galla@manchester.ac.uk

I. INTRODUCTION

The discussion whether large ecosystems can maintain stability and diversity or not has a long tradition [1–3]. While models with random interaction parameters were introduced more than 45 years ago by May [4, 5], they continue to play an important role in this diversity-stability debate. Models with random coupling coefficients are used not only for the modelling of large-scale ecosystems, but also to describe interactions in the human microbiome. For example, recent studies have examined how different types of interactions between microbe species, and between the human host and the microbes can affect stability [6, 7].

Several approaches have been taken to study the stability of ecological communities with random interaction matrices. One is concerned with assemblies with a fixed given size, S , and assumes that their interactions are set by a random matrix of size $S \times S$. These models focus on the study of the eigenvalues of the interaction matrix, but do not seek to model an actual dynamics which would generate the community of size S out of a larger pool of say N possible species. This line of approach has been taken for example in [4, 5] and in [8–13]. Knowledge and ideas from statistical physics contribute to these studies, exploiting technology developed for random-matrix problems for example in nuclear physics, the theory of disordered systems or condensed matter physics [14].

A second approach focuses on *dynamical* models of species interaction. These are often based on coupled differential equations, governing the abundances of species and their interactions. Typical examples are Lotka-Volterra equations, or closely related, replicator dynamics of evolutionary game theory. These involve a definition of reproductive fitness, which in turn requires a notion of species-to-species interaction. This is where random interaction matrices enter. One assumes for example pairwise interaction with fixed random coefficients. In the language of the theory of disordered systems this turns the problem into a dynamical problem with quenched disorder. Tools from equilibrium and non-equilibrium statistical physics can then be used to make analytical progress, usually relying on the assumption that the number of species in the system is large; formally the thermodynamic limit of an infinite number of species is taken. Different types of behaviour can then be found, both in simulations and from analytical approaches. For example dynamical systems of this type can approach stable fixed points, and in suitable parameter regimes these fixed points are found to be unique, i.e., independent of the initial condition chosen for the dynamics. For other parameters multiple fixed points or equilibria can be found. Their number and statistics can be characterised for example using Gardner-type calculations [15, 16]. Static approaches to ecosystems are based on the celebrated replica method [17–19]; this assumes the existence of a Liapunov function and typically

requires a symmetric interaction matrix.

A separate approach is based on the cavity method or the Thouless-Anderson-Palmer (TAP) equations, again originally developed in the context of spin glasses (see e.g. [20]). The focus here is not on the actual dynamics of the ecosystem, but on the statistics of fixed points, and on their stability [21–23]. The advantage relative to the replica approach is that symmetry of the interaction matrix is not required.

Finally, dynamic generating functionals (path integrals) have been used to study large ecosystems with disordered couplings. These techniques were originally developed for spin systems [24–26] (for more recent reviews see [27–29]) and then first applied to replicator dynamics by Oppen and Diederich [30], and by Berg and Weigt [16]. This was then further developed in [31–35]. The path-integral approach is dynamic, in principle, and results in an effective process for a representative species. This dynamic mean-field theory describes the time evolution of a typical degree of freedom after the average over the quenched disorder has been carried out. In most cases this effective process involves a non-Markovian retarded interaction kernel and coloured noise. This makes analytical solution difficult, in particular in transient regimes when dynamic order parameters are time dependent.

Progress can be made using the method by Eissfeller and Oppen [36] to simulate sample paths of the effective dynamics, see also [37] for further recent developments of methods to evaluate dynamical mean field theory. Analytical solutions are feasible when model parameters are such that the system converges to a unique stable fixed point, independent of the initial condition. It is then possible to derive self-consistent relations for the statistics of these fixed points and macroscopic order parameters. In the context of ecological communities these order parameters represent, among others, the fraction of species which survive in the long run, the diversity of these species (e.g., the species abundance distribution), and the overall biomass at the fixed point. The theory also self-consistently predicts its own instability, i.e. from the fixed-point solutions one can identify combinations of parameters at which dynamical instabilities set in. Outside the stable regime one then finds for example phases in which the dynamics converges to stable fixed points, but where different fixed points are reached for different starting points of the dynamics. Chaotic phases have been seen both in the context of replicator equations [31] and the learning of random games [38]. For Lotka-Volterra equations with random coupling matrices, finally, phases with unbounded growth can be identified [21–23, 39],

Most existing generating-functional studies of replicator or Lotka-Volterra models focus on cases in which the resulting effective process takes a simple form, resulting in linear fixed-point relations. These are typically models in which the (relative) growth of the abundance of one species depends linearly on the disordered fitness function. Examples can be found in [30, 31, 39]. One notable

exception are so-called Sato-Crutchfield dynamics in the context of game learning [38, 40]; in these cases the fixed point relations contain logarithmic terms in the degrees of freedom.

In this paper we focus on a further example of non-linear functional response. This is inspired by the observation that interaction between species do not grow unlimited with species abundance; instead they saturate. In ecology this is frequently modelled by so-called Holling type-II functional response [41]. This type of non-linear feedback is also known as a Hill function [42]. The aim of our work is to investigate how non-linear functional response affects the outcome of evolution of ecosystems with random interaction. Specifically we show that the truncation of feedback stabilizes communities, and leads to more diversity than in the absence of saturation.

The remainder of this paper is organized as follows. In Sec. II we define the general class of models we will be looking at, and we introduce the main control parameters. We then present results from numerical simulations of random Lotka-Volterra communities with Holling type-II functional response in Sec. III; in particular we report the different types of behaviours seen, and how the main model parameters influence this behaviour. In Sec. IV we then develop the generating functional for the model with general functional response, report the resulting effective species process, and the self-consistent equations characterising the regime of unique stable fixed points. To make further analytical progress we then focus on the case of piece-wise linear saturating functional response, and carry out a linear stability analysis. The predictions from the theory are tested in Sec. V, where we report detailed phase diagrams obtained from the path-integral analysis and from simulations. We then compare our results from the piece-wise linear feedback function to results from simulations of the model with Holling type-II functional response in Sec. VI. In Sec. VII we discuss the role of the different ecological parameters, and in particular how saturation in the functional response affects the stability of the ecosystem. We summarise our findings in Sec. VIII.

II. MODEL DEFINITIONS

We consider a pool of N species, which we label by $i = 1, \dots, N$. We write $x_i(t)$ for the abundance of species i in the ecosystem at time t . The dynamics proceed in continuous time, governed by the generalised Lotka-Volterra equations

$$\dot{x}_i(t) = r_i x_i(t) \left[K_i - x_i(t) + g \left(\sum_j \alpha_{ij} x_j(t) \right) \right]. \quad (1)$$

The quantity r_i denotes the growth rate of species i , and K_i is the carrying capacity for the species. In absence of interactions ($\alpha_{ij} = 0$ for all i, j), the abundance x_i can at most take value $x_i = K_i$.

In the following we will set $r_i = 1$ and $K_i = 1$ for all species, following [39, 43]. The coefficients α_{ij} describe the interactions between the different species. In the context of random Lotka-Volterra dynamics these are quenched disordered random variables; that is to say, they are chosen from a specified distribution at the beginning, but then remain fixed as the dynamics unfold. We will define the statistics of the α_{ij} below.

The function $g(\cdot)$ describes the ‘functional response’. Random Lotka-Volterra communities with linear functional response, $g(u) = u$, have for example been studied in [21–23, 39]. The purpose of the present work is to study non-linear functional response. We generally assume that g is a non-decreasing function of its argument.

The coefficient α_{ij} denotes the fitness benefit or detriment species i receives when interacting with species j . We set $\alpha_{ii} = 0$; self-interaction is already accounted for in Eq. (1). In our model we assume that the off-diagonal coefficients are drawn from a Gaussian distribution with the following statistics,

$$\begin{aligned}\overline{\alpha_{ij}} &= \frac{\mu}{N}, \\ \overline{\alpha_{ij}^2} - \frac{\mu^2}{N^2} &= \frac{\sigma^2}{N}.\end{aligned}\tag{2}$$

In-line with literature on disordered systems [20] we use an overbar to indicate the average over the quenched random variables $\{\alpha_{ij}\}$. Eqs. (2) indicate that the mean of each matrix element is μ/N , and their variance is σ^2/N . The scaling with N is standard in the context of disordered systems, and is chosen to guarantee a meaningful thermodynamic limit $N \rightarrow \infty$, which we will eventually assume in the generating-functional analysis.

The parameter μ controls the ‘baseline’ interaction between any pair of species. Negative values of μ indicate a generally competitive environment; the presence of any species leads to negative feedback on the growth of the other species. Similarly, if μ takes positive values, species generally interact positively with each other, and the presence of one species tends to enhance the growth of all other species. One expects this to potentially lead to unlimited growth as in [21, 22], at least in the absence of truncation effects in the functional response. We will refer to μ as the co-operation parameter.

The parameter σ describes the degree of heterogeneity in the interaction of species, we will call it the ‘heterogeneity parameter’. We also allow for correlations between the interaction coefficients α_{ij} and α_{ji} for any pair $i \neq j$ of species. Specifically, we write these as follows

$$\overline{\alpha_{ij}\alpha_{ji}} - \frac{\mu^2}{N^2} = \gamma \frac{\sigma^2}{N},\tag{3}$$

where the model parameter γ can take values between -1 and 1 . The role of the parameter γ can best be understood by considering the case $\mu = 0$. In this case $\overline{\alpha_{ij}\alpha_{ji}} = \gamma\sigma^2/N$. For $\gamma = -1$ one then finds $\alpha_{ij} = -\alpha_{ji}$ with probability one, i.e. species form predator-prey pairs; one species in each pair benefits from the presence of the other, but that other species is adversely affected by the presence of the first. For $\gamma = 0$ (and still assuming $\mu = 0$) the interaction coefficients α_{ij} and α_{ji} are uncorrelated, i.e. half of all pairs of species will be of the predator-prey type, and the other half will either both benefit from each other, or each be suppressed by the presence of the other species. For $\gamma = 1$ finally, there are no predator-prey pairs. Instead, $\alpha_{ij} = \alpha_{ji}$ with probability one, i.e. both species i and j profit from each other's presence, or the interaction is negative in both directions. If $\mu \neq 0$, the combination of α_{ij}, α_{ji} is drawn from a bivariate Gaussian distribution with non-zero mean, and the number of competitive, co-operative, and exploitative interactions can be obtained from the probabilities in the different quadrants of the α_{ij} - α_{ji} -plane. We will call γ the symmetry parameter.

The main objective of our work is to investigate how the parameters μ, σ and γ affect the outcome of the Lotka-Volterra dynamics in the presence of non-linear functional response.

III. NUMERICAL RESULTS FOR HOLLING-II FUNCTIONAL RESPONSE

We first focus on the so-called Holling type-II functional response [44, 45]. This form of feedback was originally introduced to model the rate of growth of a predator while interacting with prey; it is natural that the benefit from additional prey will eventually saturate when prey numbers are large. We extend the idea of a saturating function to all types of inter-species interactions, and study the following functional response,

$$g(u) = g_H(u) = \frac{2au}{a + 2|u|}. \quad (4)$$

The subscript H stands for Holling. For simplicity we only use one model parameter a . This function has a sigmoidal shape, and saturates to $g_H = a$ for $u \gg 1$ and to $g_H = -a$ for $u \ll -1$. We note that $g_H(u = \pm a/2) = \pm a/2$, i.e. the half-point of saturation is reached at $u = \pm a/2$.

In numerical simulations of the Lotka-Volterra system with this type of functional response we broadly find three different dynamical outcomes: In some cases the system converges to a unique fixed point. That is to say, for a fixed draw of the interaction matrix elements $\{\alpha_{ij}\}$ the dynamics converge to one single fixed point, independent of what initial conditions are used for the $\{x_i\}$. In other cases we also find fixed points, but these are no longer unique. I.e., while runs are generally found to converge, the system has multiple stable fixed-point attractors, and which one is eventually

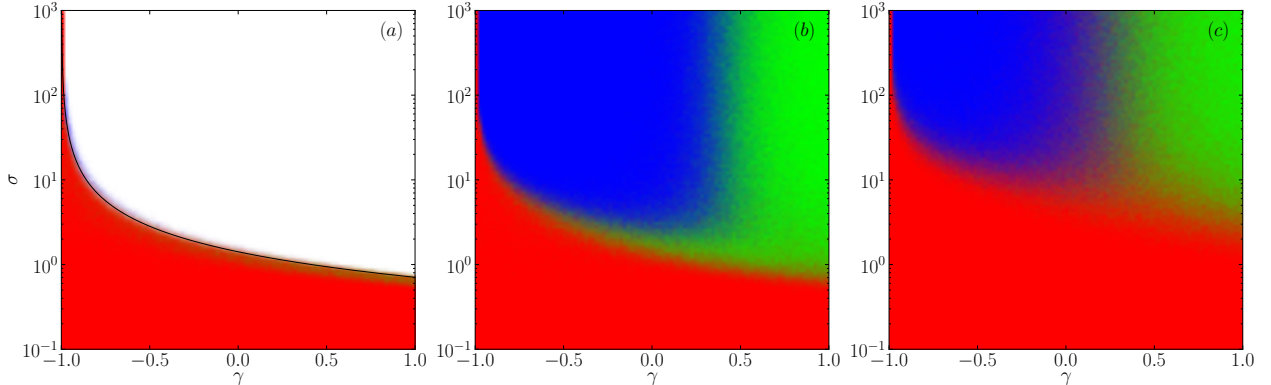


FIG. 1. Phase diagram obtained from simulations of the Lotka-Volterra system with $N = 200$. Panel (a) shows the case $a \rightarrow \infty$ (i.e., linear feedback), panels (b) and (c) are for Holling type-II functional response, with $a = 2$ in (b), and $a = 0.5$ in (c). Simulations are for $\mu = 0$. The colours indicate the dominant outcome in each part of parameter space, with red (medium gray) representing a unique stable fixed point, green (light gray) multiple fixed points, blue (dark gray) indicating parameters for which the dynamics do not converge, and white indicating unbounded growth of species abundances. The solid line in panel (a) describes the onset of instability as derived from theory (see [21, 22, 39]).

reached depends on the initial condition. The third type of outcome we find is one in which the dynamics never settles down and remains volatile until the end of the simulation. The general types of behaviour have been found previously in related systems, for example in random replicator systems, and in models of game learning [30, 31, 38].

For $a \rightarrow \infty$ we recover unrestricted linear functional response; the system can then display a fourth type of behaviour: unbounded growth [21, 22, 39]. This is due to the lack of saturation. The absence of unlimited growth for finite values of the cut-off parameter a can directly be inferred from Eq. (1). For $r_i = K_i = 1$ the relative growth rate of species i is given by $\dot{x}_i/x_i = (1 - x_i + g_i)$, where $g_i = g_H \left(\sum_j \alpha_{ij} x_j \right)$ at most takes value $g_i = a$. Thus the abundance of any species, x_i , is limited to at most $x_i = 1 + a$, as the growth rate for species i then reduces to zero. We note the difference with random replicator dynamics [17, 30, 31], in which the total abundance is constant in time ($N^{-1} \sum_i x_i = 1$) by construction, but where none of the single variables x_i is constrained to a fixed interval in the thermodynamic limit.

We present numerical simulations for the Lotka-Volterra system with Holling type-II functional response in Fig. 1. The figures illustrates the behaviour of the system in the plane spanned by the symmetry parameter γ and the heterogeneity parameter σ , for different values of the cut-off a . For each combination of these parameters we have carried out an ensemble of runs of the dynamics, and

have recorded how frequently each dynamic outcome is observed. We describe how we distinguish between the three types of behaviour in the Supplementary Information. The frequencies with which the different outcomes are found are then converted into a colour code. Red colouring (medium gray) in the figure indicates parameters for which convergence to unique fixed points is found. In the green (light gray) areas of the phase diagram, we also observe predominantly convergence to fixed points, but the system has multiple such attractors, and which one is reached depends on the initial condition. In the blue (dark gray) areas of the graphs finally we find volatile behaviour, the trajectories generated by the Lotka-Volterra system do not settle down by the end of our simulations.

We broadly find the following phase behaviour. For sufficiently small heterogeneity σ the system is stable and has a unique fixed point. This region of stability tends to be larger for low values of the symmetry parameter γ than for higher values. The presence of predator-prey pairs (anti-correlation of the matrix elements) thus promotes stability, in-line with previous observations for example in [22, 39]. If the heterogeneity σ exceeds a critical value σ_c the system either enters a phase with multiple stable fixed points, or it fails to converge. The latter tends to happen for lower values of γ , i.e. anti-correlated or moderately correlated interactions, the former for higher values of γ , when the interactions are increasingly correlated. The data in the figure shows that the saturation of the functional response stabilises the dynamics, with the stable region becoming larger for smaller values of the cut-off parameter a (i.e., for stronger non-linearity). For $a = \infty$ [panel (a) in Fig. 1] we recover the unrestricted Lotka-Volterra system with linear functional response, for which σ_c^2 is analytically known to be $\sigma_c^2 = 2/(1+\gamma)^2$ [21–23, 39]. This boundary is shown in Fig. 1(a) as a solid line. For this particular choice of parameters the system shows unlimited growth in the unstable phase (indicated in Fig. 1(a) by the absence of background shading).

We note that not all samples of the system show the same behaviour at any given set of parameters. The phase diagram in Fig. 1 shows the typical behaviour. For example some runs may converge, and others may fail to settle down before the end of the simulation. We also see trajectories which remain seemingly chaotic for a long time and then reach a fixed point only at very long times. We believe that this is due to the finite number of species, finite integration time-step, and finite run-time required in simulations, and we would expect the boundaries to become more sharp in the asymptotic limit and for infinitely large systems.

IV. GENERATING FUNCTIONAL ANALYSIS

A. Generating functional

The generating-functional analysis proceeds along the lines of [30, 31]. Starting from the dynamics in Eq. (1) one introduces the generating functional as

$$Z[\psi] = \left\langle e^{i \sum_i \int dt x_i(t) \psi_i(t)} \right\rangle, \quad (5)$$

where $\langle \dots \rangle$ denotes an average over paths of the process; this includes averaging over potentially random initial conditions (we assume that the distributions of these are independent and identical across species). The field ψ is a source term. In essence $Z[\psi]$ is the Fourier transform of the probability measure in the space of paths of the Lotka-Volterra system. The generating functional is subsequently averaged over the quenched random coupling matrix, and the thermodynamic limit, $N \rightarrow \infty$ is taken. These steps are well-established, and the calculation is lengthy. We therefore only quote the final result here. Further intermediate steps are reported in the Supplementary Material.

B. Effective representative species process

The final outcome of the path-integral analysis, after the disorder has been averaged out and the thermodynamic limit has been taken, is an effective ‘mean-field’ process for a single representative species. For the case of the Lotka-Volterra dynamics in Eq. (1) (with $r_i = 1, K_i = 1$) the effective process is of the form

$$\dot{x}(t) = x(t) \left[1 - x(t) + g \left(\mu M(t) + \gamma \sigma^2 \int_0^t dt' G(t, t') x(t') + \eta(t) \right) \right], \quad (6)$$

where one has the following self-consistent relations

$$\begin{aligned} M(t) &= \langle x(t) \rangle_*, \\ \langle \eta(t) \eta(t') \rangle &= \sigma^2 \langle x(t) x(t') \rangle_*, \\ G(t, t') &= \left\langle \frac{\partial x(t)}{\partial \eta(t')} \right\rangle_*. \end{aligned} \quad (7)$$

In these equations $\langle \dots \rangle_*$ denotes the average over realisations of the effective process, i.e., over the noise $\eta(t)$ and potentially random initial conditions. We will refer to the ‘magnetisation’ (originating from spin glass physics) $M(t)$, the correlation function $C(t, t') = \langle x(t) x(t') \rangle_*$, and the response function $G(t, t')$ as the macroscopic dynamical order parameters. In the context of ecology $M(t)$ is a measure of the biomass in the system.

C. Fixed-point analysis

We proceed to evaluate fixed points of the effective dynamics in Eq. (6). The corresponding fixed-point relations are

$$x^* [1 - x^* + g(\mu M^* + \gamma \sigma^2 \chi x^* + \eta^*)] = 0 \quad (8)$$

where we have used the superscript $*$ to indicate quantities evaluated at the fixed point. In the fixed-point regime one has $G(t, t') = G(t - t')$ (time translation invariance), and we have introduced the integrated response $\chi = \int_0^\infty d\tau G(\tau)$. The correlation function $C(t, t') = \langle x(t)x(t') \rangle_*$ becomes independent of t and t' at the fixed point, and we write $q \equiv C(t, t')$. We can then replace η^* by $\eta^* = \sigma\sqrt{q}z$, where z is a static Gaussian random variable of mean zero and with variance one.

Eq. (8) always has the solution $x^*(z) = 0$ for all z . Potential other solutions fulfill the relation

$$x^* = 1 + g(\mu M^* + \gamma \sigma^2 \chi x^* + \sigma\sqrt{q}z) \quad (9)$$

Such solutions are only physically valid provided they are non-negative, as x^* describes the abundance of an effective species.

It is difficult to proceed analytically for general choices of the function g . In particular, if g is non-linear Eq. (9) would have to be solved numerically for $x^*(z)$ for a given value of z . We therefore consider a piece-wise linear feedback function g . Specifically, we follow [46] and approximate the Holling type-II response by

$$g(u) = g_P(u) = \begin{cases} a & u \geq a \\ u & -a \leq u \leq a \\ -a & u \leq -a. \end{cases} \quad (10)$$

The subscript g_P refers to piece-wise linear. This function is linear in u in the interval $-a \leq u \leq a$, and is then ‘clipped’. Similar to the Holling type-II response the function saturates at a for large u , and at $-a$ for large negative values of u . We also note that $g(a/2) = a/2$, i.e., the saturation half-point of the piece-wise linear model is the same as for the Holling type-II functional response in Eq. (4). This structure allows us to proceed with the mathematical analysis, and at the same time it conserves some of the main features of the Holling type-II system as we will discuss further below.

To find the solution $x^*(z)$ of Eq. (9) we consider the three branches of $g_P(u)$. These are separated by threshold values z_1 and z_2 for the static noise variable z ; we will evaluate these thresholds below. Specifically, we find:

- (i) For $z \geq z_2$, the argument of the function g_P exceeds a and hence $g_P(u) = a$; this gives the solution $x^*(z) = 1 + a$;
- (ii) For $z_1 \leq z \leq z_2$ one has $g_P(u) = u$, giving $x^*(z) = \frac{1+\mu M^*+\sigma\sqrt{q}z}{1-\gamma\sigma^2\chi}$;
- (iii) For $z \leq z_1$ finally, the value $x^*(z)$ depends on the choice of the cut-off a in the following way: if a is smaller than the carrying capacity (i.e., $a \leq 1$), the response saturates at $g_P = -a$, and we find $x^*(z) = 1 - a$. If $a \geq 1$, the (effective) species dies out, $x^*(z) = 0$, before the response reaches saturation.

The threshold values z_1 and z_2 are found from the argument of the function g in Eq. (9),

$$\begin{aligned} z_1 &= \frac{(1-a)(1-\gamma\sigma^2\chi)\Theta(1-a) - (1+\mu M^*)}{\sigma\sqrt{q}}, \\ z_2 &= \frac{(1+a)(1-\gamma\sigma^2\chi) - (1+\mu M^*)}{\sigma\sqrt{q}}. \end{aligned} \quad (11)$$

In the first expression $\Theta(\cdot)$ is the Heaviside step function, used here to differentiate between the cases $a \geq 1$ and $a \leq 1$. A more detailed discussion can be found in Sec. S1 H of the Supplementary Information.

Putting the different cases together we find the following physical fixed-point value for a given combination of z and a ,

$$x^*(z) = \begin{cases} 1 + a & z \geq z_2, \\ \frac{1+\mu M^*+\sigma\sqrt{q}z}{1-\gamma\sigma^2\chi} & z_1 \leq z \leq z_2, \\ (1-a)\Theta(1-a) & z \leq z_1. \end{cases} \quad (12)$$

We note that the abundance x^* of the effective species is bounded from above by $1 + a$. This indicates that, unlike in standard Lotka-Volterra dynamics, abundances cannot diverge, and hence the average species population given by the order parameter M^* also remains finite. The lower bound for the solutions of Eq. (9) is zero for $a \geq 1$, and given by $1 - a$ for $a \leq 1$.

It is important to recall that $x^*(z) = 0$ is a solution of the fixed-point equation (8) for all z . However, we find in linear stability analysis that this zero solution is an attractor only when $a \geq 1$ and $z \leq z_1 = -\frac{1+\mu M^*}{\sigma\sqrt{q}}$, i.e. only when $x^*(z) = 0$ is the unique solution of the fixed point equation (8). This is shown in Sec. S1 I of the Supplementary Material. For $a < 1$, the solution $x^* = 0$ cannot be realised, and all species in the initial pool will have non-zero abundances in the phase of unique stable fixed points.

Using Eq. (12) we can write Eqs. (7) in the following form

$$M^* = \int_{z_2}^{\infty} (a+1) Dz + \int_{z_1}^{z_2} \frac{1 + \mu M^* + \sigma \sqrt{q} z}{1 - \gamma \sigma^2 \chi} Dz + \Theta(1-a) \int_{-\infty}^{z_1} (1-a) Dz, \quad (13a)$$

$$q = \int_{z_2}^{\infty} (a+1)^2 Dz + \int_{z_1}^{z_2} \left(\frac{1 + \mu M^* + \sigma \sqrt{q} z}{1 - \gamma \sigma^2 \chi} \right)^2 Dz + \Theta(1-a) \int_{-\infty}^{z_1} (1-a)^2 Dz, \quad (13b)$$

$$\chi = \frac{1}{1 - \gamma \sigma^2 \chi} \int_{z_1}^{z_2} Dz, \quad (13c)$$

where we have introduced the shorthand $Dz = \frac{dz}{\sqrt{2\pi}} e^{-z^2/2}$ for the Gaussian measure of z .

Together with Eqs. (11) this is a self-consistent set of relations for the order parameters q, χ and M^* in the regime of unique stable fixed points. Solutions of these equations can be obtained numerically as function of the model parameters μ, σ, γ and a . The method we use to solve this set of equations is described in the Supplementary Material.

D. Linear stability analysis

We now carry out a linear stability analysis of the fixed points identified in the previous section. We first notice that fixed points of the form $x^*(z) = 1 + a$, $x^*(z) = (1-a)\Theta(1-a)$ are always locally stable. This is shown in Section S1 I in the Supplementary Material.

We note that the function $g(\cdot)$ is the identity function in the vicinity of the remaining fixed points. We write $x(t) = x^* + y(t)$ and $\eta(t) = \sigma \sqrt{q} z + v(t)$, and following [17] we add noise of zero mean and unit amplitude $\xi(t)$ in the effective process to study stability.

Linearising the effective dynamics in Eq. (6) in y and v we find

$$\dot{y}(t) = x^* \left(-y(t) + \gamma \sigma^2 \int_0^t dt' G(t-t') y(t') + v(t) + \xi(t) \right). \quad (14)$$

Carrying out a Fourier transform, this can be written as

$$\frac{i\omega \tilde{y}(\omega)}{x^*} = \left(\gamma \sigma^2 \tilde{G}(\omega) - 1 \right) \tilde{y}(\omega) + \tilde{v}(\omega) + \tilde{\xi}(\omega). \quad (15)$$

Following [30, 31] we now focus on the long-time behaviour of perturbations, i.e., on the mode at $\omega = 0$; see also [29]. Re-arranging Eq. (15) and taking averages we find

$$\langle |\tilde{y}(0)|^2 \rangle = \phi \frac{\langle |\tilde{v}(0)|^2 \rangle + 1}{(1 - \gamma \sigma^2 \chi)^2}, \quad (16)$$

where the factor $\phi = \int_{z_1}^{z_2} Dz$ accounts for the fact that Eq. (14) only applies to fixed points for which g is not saturated, i.e. for values of z with $z_1 \leq z \leq z_2$. Finally, using the self-consistency relation $\langle |\tilde{y}(0)|^2 \rangle = \sigma^2 \langle |\tilde{v}(0)|^2 \rangle$, we find

$$\langle |\tilde{y}(0)|^2 \rangle = \frac{\phi}{(1 - \gamma \sigma^2 \chi)^2 - \phi \sigma^2}. \quad (17)$$

This quantity is finite (and non-negative) in the phase of stable fixed points, and becomes infinite when

$$\phi = \frac{(1 - \gamma\sigma^2\chi)^2}{\sigma^2}. \quad (18)$$

This condition signals the onset of instability.

V. TEST AGAINST SIMULATIONS AND PHASE DIAGRAM

A. Species abundance distributions

We first discuss the resulting species abundance distributions in the regime of unique stable fixed points (i.e., the distribution of the $\{x_i\}$). In Fig. 2 we show examples of species abundance distributions for different values of σ and γ for $a = 0.5$ and $\mu = 0$. The shaded histograms in the figures are from simulations, solid black lines indicate the distributions of the unsaturated species from the theory. On the left of each of the figure [panels (a), (e), (i)] we show how z_2 (upper line) and z_1 (lower line) vary with increasing heterogeneity σ .

To interpret the histograms in Fig. 2 we note that the weight of each branch of the solution in Eq. (12) is equal to the probability of a standard Gaussian random number z to fall between or on either side of z_1 and z_2 , respectively. For $\sigma = 0$, there is no species heterogeneity ($\alpha_{ij} = 0$ for all i, j); all species abundances take the value $x^* = M^*$, where $M^* = 1/(1 - \mu)$ from Eq. (13a). One finds $z_1 \rightarrow -\infty$ and $z_2 \rightarrow \infty$, and the functional response does not reach saturation.

For non-zero values of the interaction strength σ , z_1 and z_2 become finite; as a consequence there is a finite probability of z falling outside the interval $[z_1, z_2]$, and hence the functional response saturates for a finite fraction of species. This results in a clipped Gaussian distribution for x^* ; the fraction of species in the clipped regions increases with σ .

We find that both z_1 and z_2 are decreasing functions of γ , this is consistent with Eqs. (11), where the explicit factor of γ dominates over the dependence of M^* , q and χ on γ .

As a consequence the proportion of species ‘clipped off’ at either side changes as γ varies. We find a lower mean species abundance M^* , and more species at $1 - a$ than at $1 + a$ for $\gamma = -1$, and a higher mean abundance with more species at the upper bound $1 + a$ for $\gamma = 1$.

We find similar results for $a = 2$; these are shown in Fig. S1 in the Supplementary Material. As the limiting values ($x^* = 0$ and $x^* = 1 + a$) for the species abundances are further apart for this case, a higher value of σ is required to spread the abundance distribution to these values. Therefore we find less saturation for $a = 2$ than for $a = 0.5$ at a fixed value of the heterogeneity parameter σ .

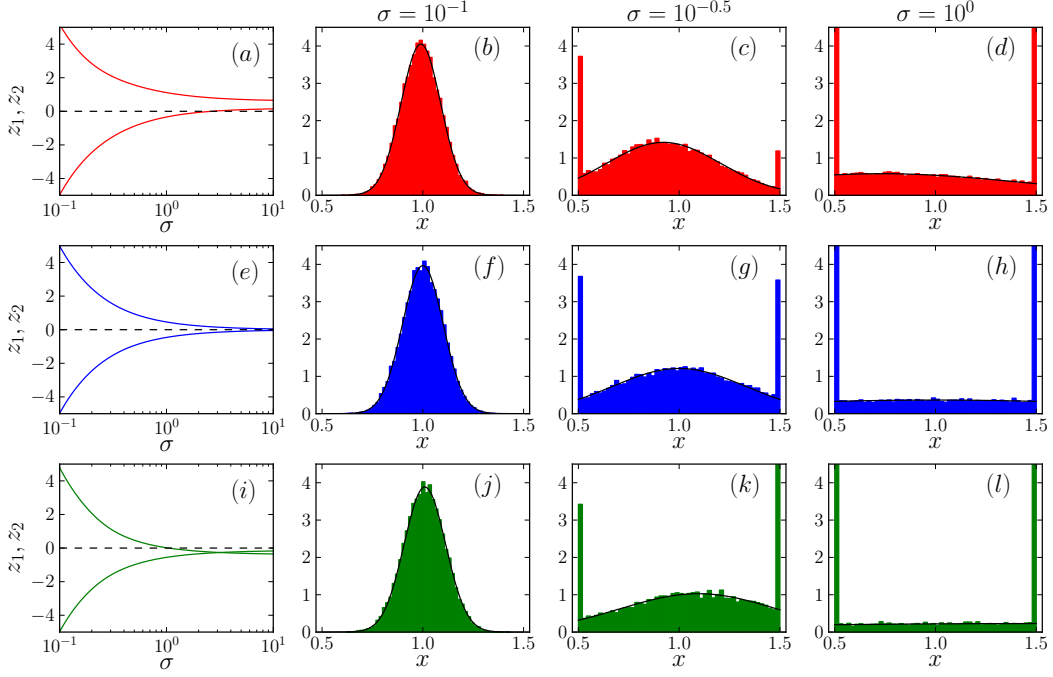


FIG. 2. Species abundance distribution for the case $a = 0.5$ and $\mu = 0$ for different values of the heterogeneity parameter σ . The upper row [panels (a)-(d)] is for $\gamma = -1$, the middle row [(e)-(h)] for $\gamma = 0$, and the lower row [(i)-(l)] for $\gamma = 1$. On the left [(a),(e),(i)] we show z_2 (upper line) and z_1 (lower line), remaining panels show the species abundance distributions, for $\sigma = 10^{-1}$ [(b),(f),(j)], $\sigma = 10^{-0.5}$ [(c),(g), (k)] and $\sigma = 1$ [(d),(h),(l)]. Solid lines are theoretical predictions for the species abundance distribution, shaded histograms are from simulations.

B. Test of theoretical predictions for order parameters at stable fixed points

The analytical theory results in predictions for the order parameters q , χ and M^* as a function of the model parameters a , μ , γ and σ . These predictions are obtained as the solutions of the coupled equations (13a,13b,13c). They are valid in the parameter regime in which the Lotka-Volterra system converges to a unique stable fixed point, independent of initial conditions.

A comparison of theory and simulation is shown in Fig. 3. Theoretical predictions are indicated by solid lines, results from simulations as symbols. We show the quantities ϕ , M^* and a measure of diversity related to Simpson's index. Simpson's index [47] is the probability that two randomly chosen individuals in the community are of the same species, $\mathcal{S} = \sum_i \left(\frac{x_i}{\sum_j x_j} \right)^2$. For our model this index is given by $\mathcal{S} = q/(NM^2)$. A low value of this probability indicates high diversity of species; therefore the inverse Simpson index, $\mathcal{S}^{-1} = NM^2/q$ characterizes the diversity of the ecological community. The diversity scales linearly with N ; therefore we report the relative diversity $\mathcal{S}^{-1}/N = M^2/q$. A

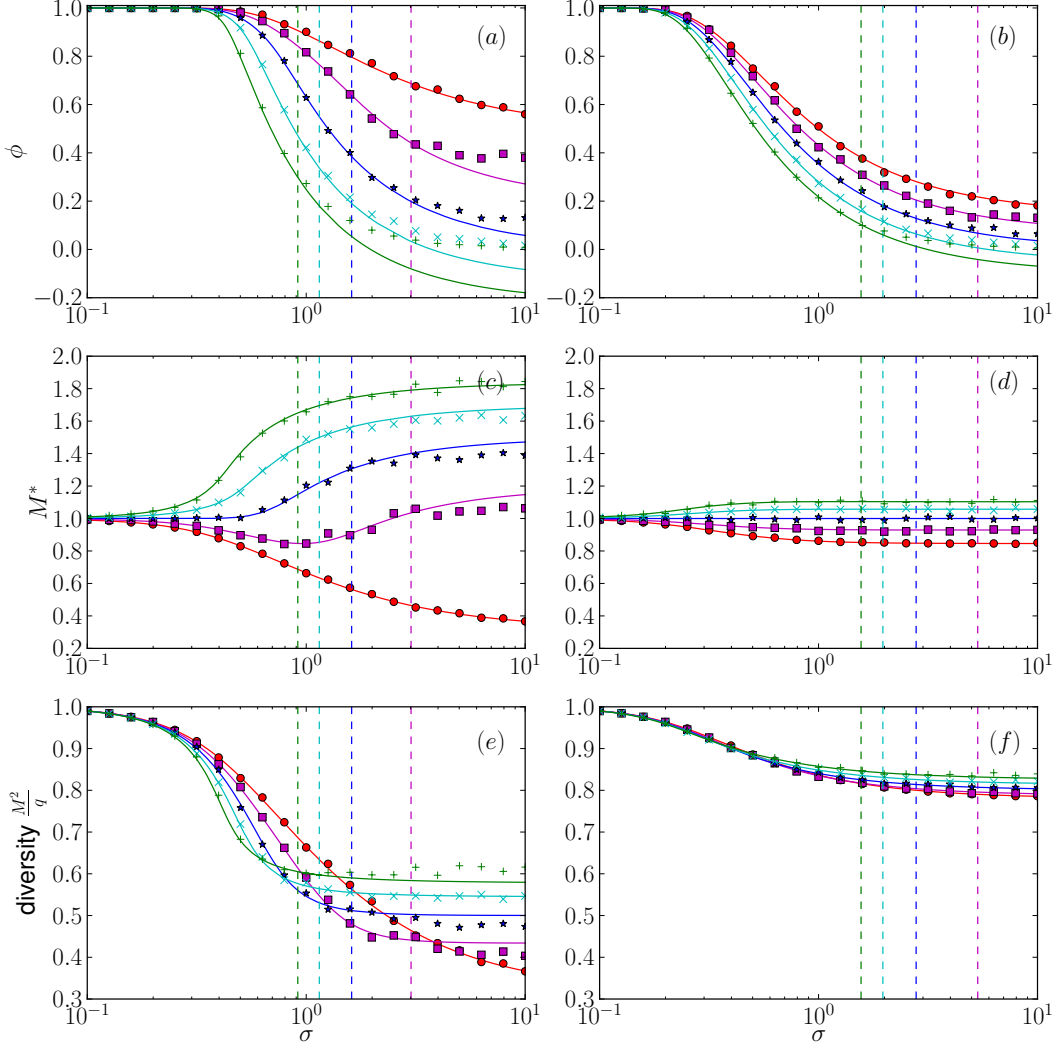


FIG. 3. Comparison of theoretical predictions (lines) for the characteristic order parameters against simulations (points). Data is for $\mu = 0$, $\gamma = -1$ (●), -0.5 (■), 0 (★), 0.5 (×), and $\gamma = 1$ (+). This is for the model with piece-wise linear functional response. Left-hand column [(a),(c),(e)] is for $a = 2$, right-hand column [(b),(d),(f)] for $a = 0.5$. The vertical dashed lines mark the onset of instability as predicted by the theory; analytical predictions can no longer be expected to match with simulations in the unstable phase to the right of the dashed lines. The graphs show the fraction of species not saturated ϕ , the biomass M^* , and the diversity M^2/q as functions of σ .

more detailed explanation of how these quantities were measured from simulations and predicted from the theory can be found in the Supplementary Material.

The vertical dashed lines in Fig. 3 indicate the predicted onset of instability. More precisely unique stable fixed points are predicted for small values of σ , i.e., to the left of the dashed lines. To the right of these lines the system either has multiple fixed points, or never settles down, and

in either of these scenarios the analytical predictions for the stable fixed point phase can no longer be expected to apply. The figure indicates agreement between theory and simulation in the stable phase. Systematic deviations can be found in the unstable regime, although the predictions from the theory appear to remain a good approximation in some cases. Similar observations have been made in related models, see e.g. [22, 31].

We note that solving Eqs. (13) can lead to $z_1 > z_2$ in the unstable phase. This results in the prediction of a negative value of ϕ (the fraction of unsaturated species), which demonstrates further that the theory does not apply in this parameter regime.

The biomass in the population, M^* , tends to higher values for positive values of the symmetry parameter γ , i.e., in absence of exploitative interactions and predator-prey pairs. This is shown in panel (c) in Fig. 3.

This can be understood from the species abundance distributions in Fig. 2, and from the dependence of this distribution on γ . We find more species with larger abundances for positive γ , and more species with smaller abundances for negative γ . This is due to the dependence of z_1 and z_2 on γ as discussed in Sec. V A.

These effects are reduced for stronger non-linearity, as shown in Fig. 3(d). Generally, we find that a lower value of the cut-off parameter a reduces the dependence of the order parameters on γ . We also note that a much higher diversity of species is maintained for lower cut-off thresholds [c.f. Fig. 3(e) and (f)]

C. Onset of instability

In Fig. 4 we investigate the onset of instability in more detail. We use several indicators to detect different types of behaviour in the numerical solutions of the Lotka-Volterra equations. In order to characterise the (relative) variation of species abundances over time, we calculate

$$h = \frac{\left\langle \left\langle x_i(t)^2 \right\rangle_t - \left\langle x_i(t) \right\rangle_t^2 \right\rangle_N}{\left\langle \left\langle x_i(t) \right\rangle_t^2 \right\rangle_N}. \quad (19)$$

In this expression $\langle \dots \rangle_t$ indicates an average over time; this is taken in the stationary state; reported values are time averages over the last 1% of trajectories (numerical integration of the Lotka-Volterra equations is carried out up to final time $t_f = 200$). The notation $\langle \dots \rangle_N$ in Eq. (19) denotes an average over species, $\langle \dots \rangle_N = N^{-1} \sum_i \dots$. The order parameter h indicates whether or not the system settles down to a fixed point: when $h = 0$ a fixed point is reached eventually, whereas positive values of h indicate persistent volatile dynamics. In order to identify the phase with multiple fixed

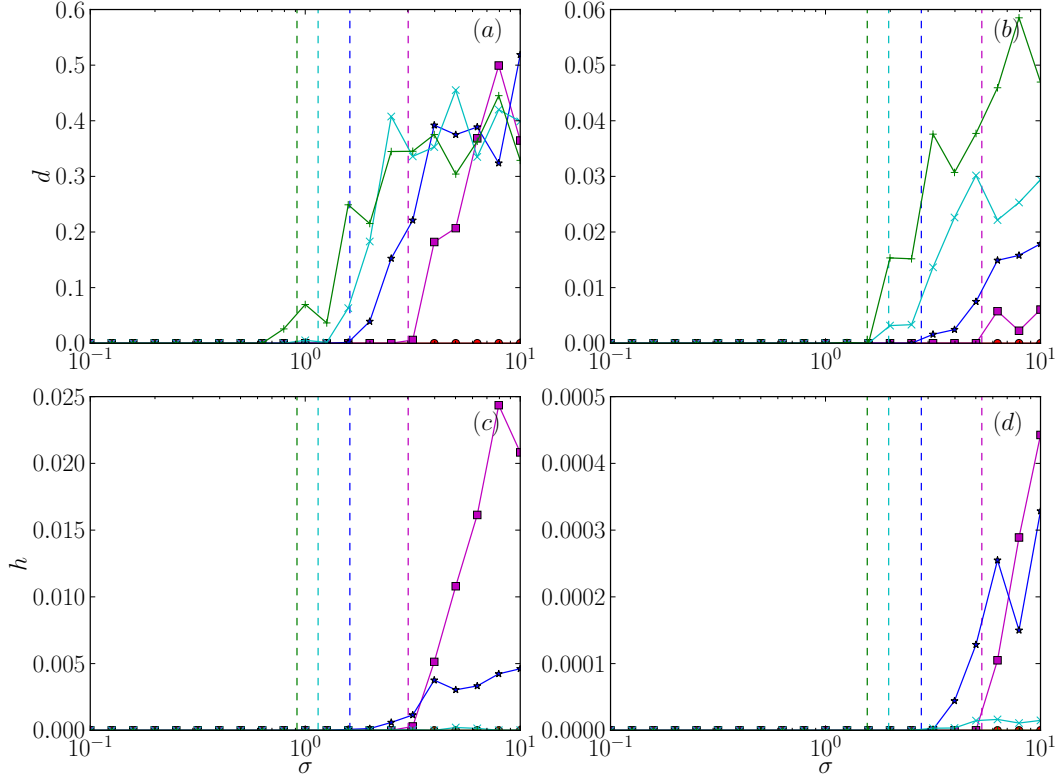


FIG. 4. Onset of instability for the model with piece-wise linear functional response. Left-hand column [(a),(c)] is for $a = 2$, right-hand column [(b),(d)] for $a = 0.5$. The vertical dashed lines mark the onset of instability as predicted by the theory. The graphs show d (top) and h (bottom). Data is for $\mu = 0$, and $\gamma = -1(\bullet)$, $-0.5(\blacksquare)$, $0(\star)$, $0.5(\times)$, $1(+)$.

points, we have additionally run the following numerical experiments. For a fixed realisation of the interaction matrix we have generated two independent random initial conditions. We then run each of these separately, and compute the relative distance

$$d = \left\langle \frac{\langle (x_i - x'_i)^2 \rangle_N}{\langle x_i \rangle_N^2} \right\rangle_t, \quad (20)$$

where x_i and x'_i are the trajectories for the two sets of initial conditions. This quantity is again evaluated in the stationary state. Thus, $d \approx 0$ when the asymptotic behaviour is independent of initial conditions, and $d > 0$ otherwise.

The data shown in the upper panels of Fig. 4 shows that $d \approx 0$ for small heterogeneity σ independently of the symmetry parameter γ , but that a phase with dependence on initial conditions is found when the stability threshold is crossed ($\sigma > \sigma_c$). The results in the lower panels of Fig. 4 indicate that the dynamics remains volatile ($h > 0$) for large values of σ when the symmetry parameter is zero or moderately negative. The figure shows that a fixed point is almost certainly reached for $\gamma = 1$

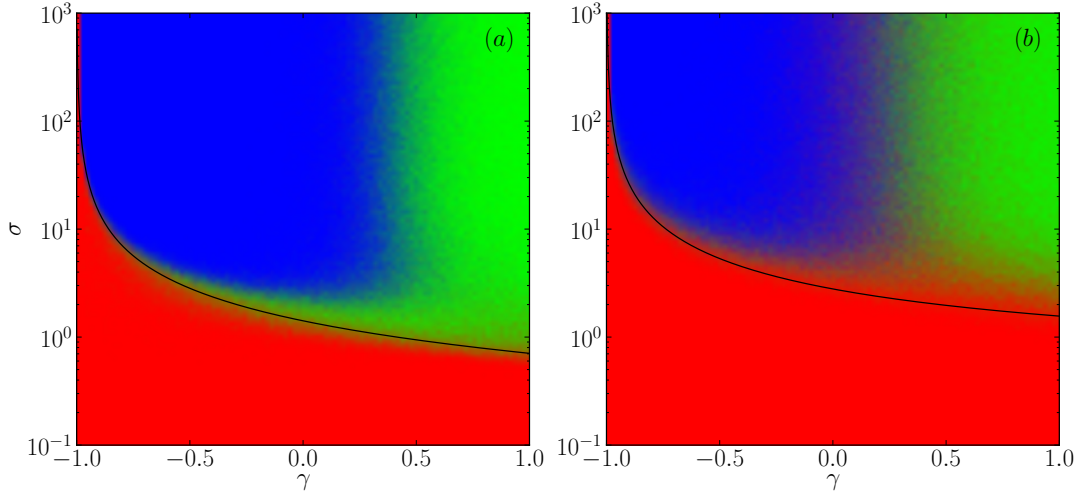


FIG. 5. Phase diagram obtained from simulations of the Lotka-Volterra systems with piece-wise linear functional response with $N = 200$. As in Fig. 1 the colours (gray shading) indicate the dominant outcome in each part of parameter space [red (medium gray): unique stable fixed point; green (light gray): multiple fixed points; blue (dark gray): dynamics do not converge]. Solid black lines show the onset of instability as predicted from the generating-functional approach. Data is for $\mu = 0$, panel (a) for $a = 2$, panel (b) for $a = 0.5$.

and is likely to be reached for $\gamma = 0.5$, although these fixed points are not unique.

Comparing the scales of the left and right hand panels in Fig. 4 shows that the order parameters d and h are much smaller for the lower value of the cut-off a ; this is due to the tighter bounding effect of the functional response.

VI. COMPARISON OF LOTKA-VOLTERRA SYSTEMS WITH HOLLING TYPE-II AND PIECE-WISE LINEAR FUNCTIONAL RESPONSE

A. Phase diagram and onset of instability

In Fig. 5 we show examples of the phase diagram obtained from numerical integration of the Lotka-Volterra system with piece-wise linear response. These are generated in the same way as in Fig. 1. Red (medium gray) indicates parameter values of the phase with unique fixed points, green (light gray) indicates multiple fixed points, and blue (dark gray) indicates volatile behaviour. The black line in each panel shows the boundary, σ_c , of the phase with a unique stable fixed point, predicted by the theory. As seen in the figure the theory is in agreement with results from numerical integration of the Lotka-Volterra system. We attribute remaining minor discrepancies to finite integration time, finite time steps, and finite species number.

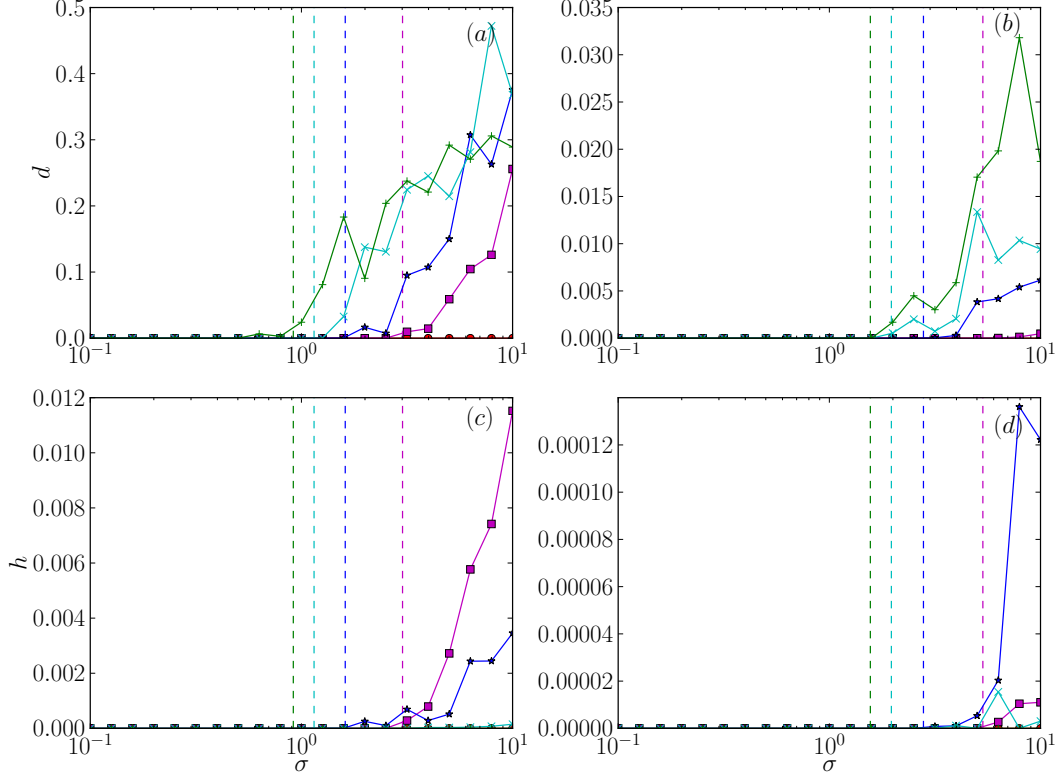


FIG. 6. Onset of instability for Holling type-II functional response. Left-hand column [(a),(c)] is for $a = 2$, right-hand column [(b),(d)] for $a = 0.5$. The vertical dashed lines mark the onset of instability predicted for the piece-wise feedback function from theory. The graphs show d (top) and h (bottom). Data is for $\mu = 0$, $\gamma = -1(\bullet)$, $-0.5(\blacksquare)$, $0(\star)$, $0.5(\times)$, $1(+)$.

Comparing Figs. 1 and 5, we find that the behaviour of the systems with Holling type-II and piece-wise linear functional response are very similar. Unique fixed points are reached for values of σ below a critical point for all values of the symmetry parameter γ , with much higher critical values σ_c for lower γ . This indicates higher stability for asymmetric couplings than in the symmetric case. Above this critical value of the heterogeneity parameter we find multiple fixed points for positively correlated interactions, and persistent volatile behavior, such as limit cycles or chaos for negatively correlated couplings. In both Fig. 1 and Fig. 5, one notices the stabilising effect of a lower value of the cut-off parameter a in the functional response, i.e., for smaller a one finds a larger red (medium gray) area indicating stable unique fixed points, and higher critical values for σ .

In order to make the comparison between the two models more precise we report results for the order parameters h and d from numerical simulations of the model with Holling type-II functional response in Fig. 6, along the analytical prediction for the onset of instability in the model with piece-wise linear response. The data shows that the system with Holling type-II response has very

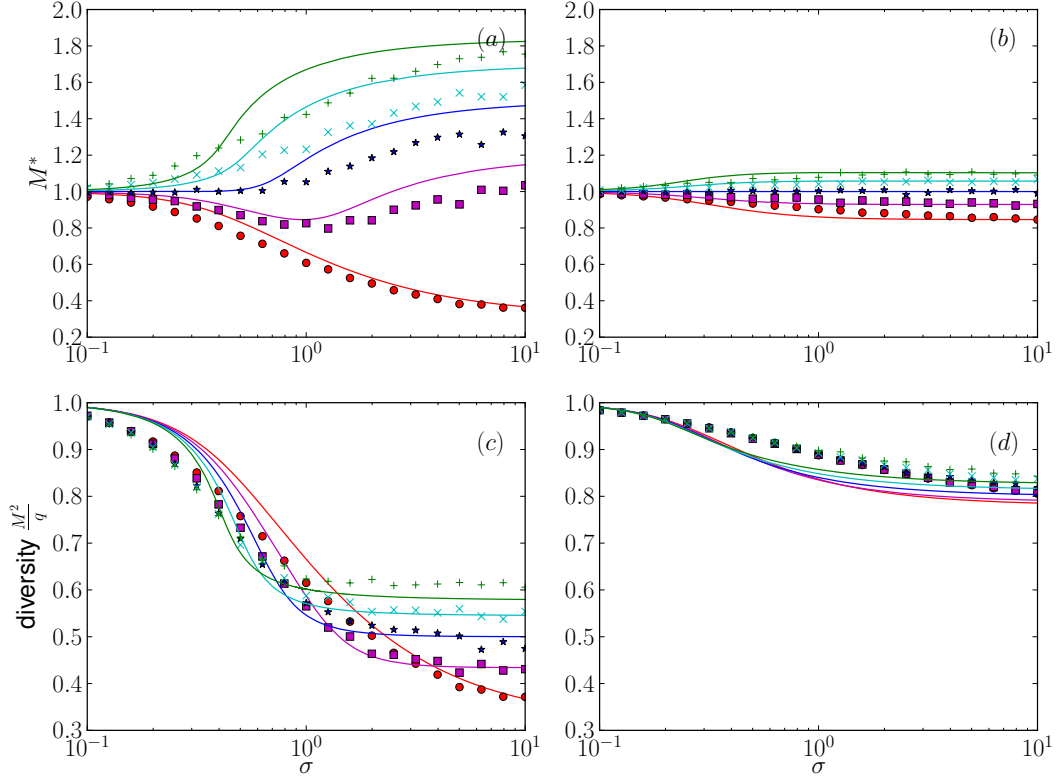


FIG. 7. Comparison of theoretical predictions for M^* and diversity for the piecewise functional response (lines) against simulations for Holling type-II functional response (points). Left-hand column [(a),(c)] is for $a = 2$, right-hand column [(b),(d)] for $a = 0.5$. Data is for $\mu = 0$, $\gamma = -1(\bullet)$, $-0.5(\blacksquare)$, $0(\star)$, $0.5(\times)$, $1(+)$.

similar behaviour as that with the piece-wise linear feedback. We find volatile dynamics for anti-correlated interactions past the critical interaction strength, and multiple fixed points for correlated interactions. The point at which h and d become non-zero is very close to the onset of instability predicted by the theory for the model with piece-wise linear feedback.

B. Order parameters in the stable phase

In Fig. 7 we compare results from numerical integration of the Lotka-Volterra equations with Holling type-II functional response (markers), with the analytical solutions for piece-wise linear response (lines). As seen in the figure the general behaviour of the biomass M^* and diversity as functions of σ and γ are similar in both models.

The main difference between the piece-wise linear function and the Holling type-II function is how they approach their upper and lower limits $\pm a$. The piece-wise linear function $g_P(u)$ approaches its limits linearly, and attains them at $u = \pm a$ [$g_P(\pm a) = \pm a$]; the sigmoidal Holling function g_H

approaches the limits much more slowly, and only attains them asymptotically. As a consequence, we have $|g_H(u)| < |g_P(u)|$ for $|u| > a/2$. The differences in the two functions account for the differences we see between the results in Fig. 7. We find the order parameters M^* and diversity to display a much smoother dependence on heterogeneity for the Holling function (markers) than for the piece-wise function.

For the larger values of σ shown in Fig. 7(a), we find that M^* is lower for the Holling function for all values of γ . For $a = 2$ species die before they can saturate to the lower boundary. In this case the difference in saturation is therefore only present at the upper limit, and this results in lower values of M^* for the Holling function. This is because species are closer to upper saturation for higher values of σ , where the Holling type-II function is lower in magnitude than the piece-wise linear function. The lower value of the Holling function causes these species to have lower abundances than in the piece-wise case.

For $a = 0.5$, species are able to reach both saturation points before they can die, therefore the difference in the two response functions affects the species both at the upper and lower boundaries. As a consequence, we do not see the same consistent effect of lower M^* as we did in the case of $a = 2$, see Fig. 7(b).

In the limit of infinite σ , both the Holling and piece-wise linear function are equal. This results in the values of M^* to tend to the same limit in both models, and similarly for the diversity. In this limit all species abundances will be saturated at either boundary, $x_i = 1 + a$ or $x_i = (1 - a)\Theta(1 - a)$. The fraction of species saturated at each boundary is the same for either function, for a given γ . This results in the same limiting values for the order parameters M^* and diversity in both models.

VII. DEPENDENCE OF STABLE REGION MODEL PARAMETERS

In the previous section we compared results from analysis and simulations of the piece-wise linear functional response to demonstrate that our theory correctly predicts the nature of the system in the regime of unique fixed points, see Fig. 3. The theory also correctly predicts the critical value of σ where this regime ends, as demonstrated in Fig. 4. We then compared predictions for the model with piece-wise linear response with simulation results for the model with Holling type-II feedback. We found a similar general dependence of the system's order parameters on σ , γ , and a , see Fig. 7. The onset of instability, σ_c is also very similar on both models, as shown in Fig. 6. We conclude that the predictions of our theory for the piece-wise linear feedback function are a good approximation to the behaviour of the model with Holling type-II functional response. It is therefore appropriate

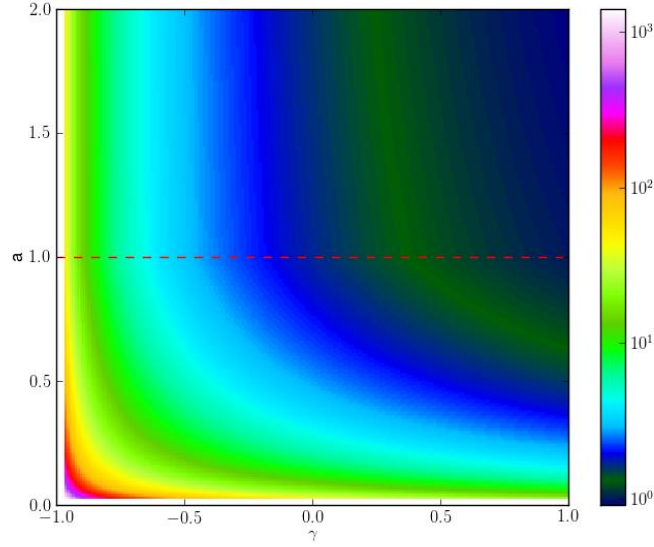


FIG. 8. Critical value of the heterogeneity parameter, σ_c , plotted as a colour map in the a - γ plane at fixed $\mu = 0$. Higher values of σ_c indicate higher stability. The dashed line indicates $a = 1$ (cut-off equal to carrying capacity), see text for further discussion.

to use the theory we have developed to investigate further how the stability of the ecosystem with saturating functional response depends on the key model parameters.

A. Dependence of stability on the cut-off parameter a

We have so far shown results only for $a = 2$ and $a = 0.5$. These fall on either side of the carrying capacity which was set to one. In Fig. 8 we provide a more general picture, and show how the critical value of the heterogeneity, σ_c , depends on the cut-off a , and on the symmetry parameter γ . In this figure we fix the mean value μ of the interaction matrix elements.

As one would expect, the range of the stable region increases as the functional response becomes more restricted (i.e., as a is lowered). This effect is particularly relevant when the cut-off is lower than the carrying capacity (i.e., for $a < 1$). We note that in this regime the critical strength of the heterogeneity is a decreasing function of both a and γ . For $\gamma < 0$ we also note that the stability has a similar dependence on the two parameters a and γ , which is demonstrated by the symmetry in the bottom left quadrant of Fig. 8. If the cut-off parameter a exceeds the carrying capacity ($a > 1$), its influence on the size of the stable region is small.

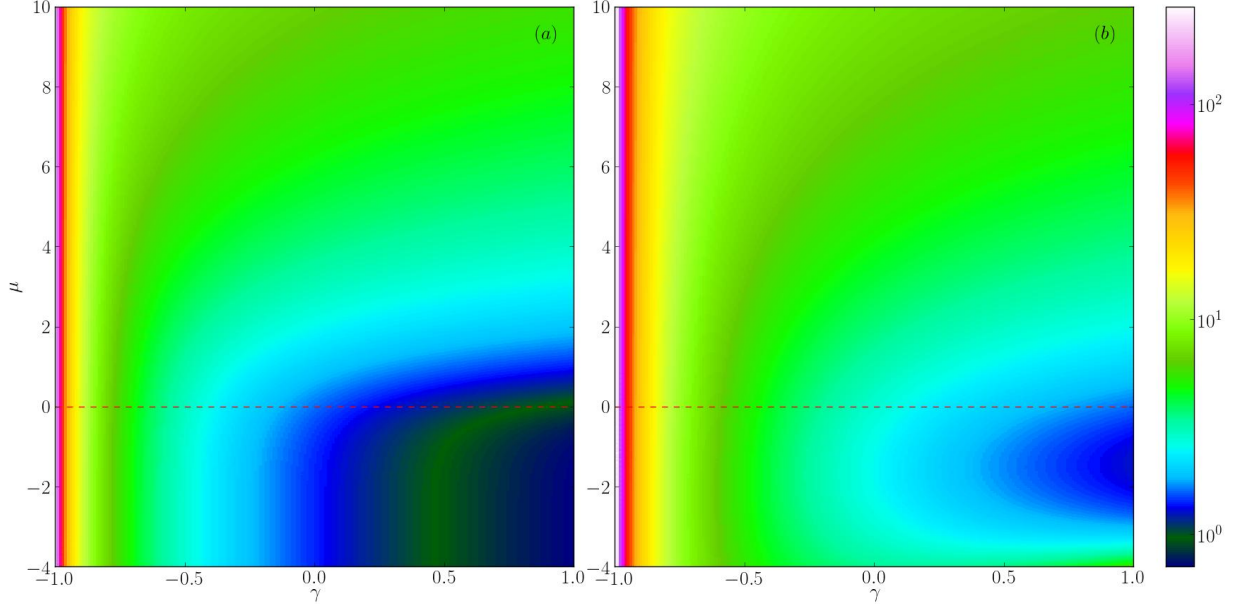


FIG. 9. Critical σ_c plotted as a colour map in the μ - γ plane at fixed $a = 2$ (left) and $a = 0.5$ (right). Higher values of σ_c indicate higher stability. The data along the dashed line indicates values of σ_c for $\mu = 0$, these are as previously given in the black lines of Fig. 5.

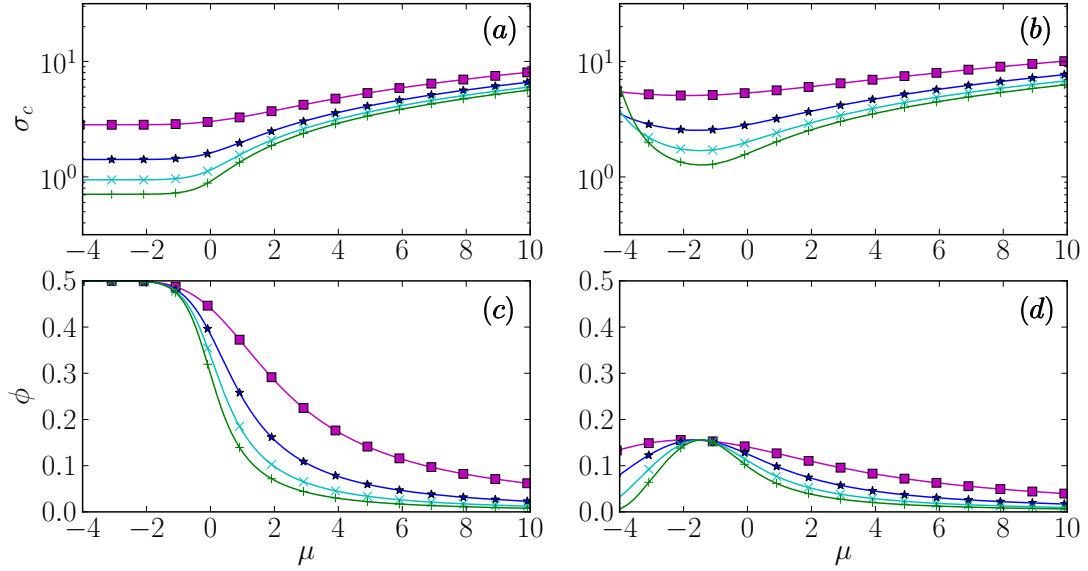


FIG. 10. Location of the onset of instability σ_c , and fraction of unsaturated species, ϕ , for varying μ at $a = 2$ (left) and $a = 0.5$ (right). Results in the figure are from the theory, the different values for γ are indicated by different symbols [$\gamma = -0.5$ (\blacksquare), 0 (\star), 0.5 (\times), 1 ($+$)].

B. Dependence of stability on cooperation parameter μ

We have not yet considered how stability varies with the co-operation parameter μ , i.e., on the mean interacting strength between species. In the context of gut bacteria it has been argued that increasing the co-operation between species of an ecological system can reduce the system's stability [6], with higher stability found for more competitive systems. Previous theoretical studies [21, 22, 35] of random Lotka-Volterra systems without functional response have found σ_c to be independent of μ so long as $\mu \leq 0$. We note that the interaction term between the species carries the opposite sign in [21, 22] relative to our notation, implying opposite sign conventions in particular for the parameter μ . In [21, 22] a second critical value of the heterogeneity is found; if the strength of the heterogeneity exceeds this value, the system displays unbounded growth. This value is found to depend on μ , and to be equal to zero for $\mu \geq 1$; that is to say, when $\mu > 1$ the random Lotka-Volterra system with linear functional response always exhibits unbounded growth regardless of the amount of heterogeneity.

The saturated functional response in our model causes the abundances to be constrained to the interval $1 - a\Theta(1 - a) \leq x_i(t) \leq 1 + a$, and as a consequence the system cannot display unbounded growth. The critical value for σ however, is now dependent on the value of μ . In Fig. 9 we show how σ_c varies with μ and γ for $a = 2$ and $a = 0.5$; these results are from numerical evaluation of the self-consistency equations obtained from the generating functional analysis.

We first discuss the case $a = 0.5$. We find a minimum value for σ_c as a function of μ , see the lower right corner of Fig. 9(b). This minimum value corresponds to a maximum proportion of unsaturated species ϕ , this is shown in S1 J and demonstrated in Fig. 10. For values of μ away from this extremal point, ϕ decreases as more species become saturated at either $1 + a$ (increasing μ) or $1 - a$ (decreasing μ), this in turn gives the system a higher stability.

For $a = 2$ we also find increasing stability for higher values of μ . However, we do not find a minimum point for stability (as a function of μ). Instead σ_c monotonically decreases with decreasing μ , tending to a constant. This is because the fraction of species at the lower saturation point ($x^* = 0$ for $a = 2$) does not increase past 0.5 as μ is decreased. These results are different to those found in [6], where a model with linear functional response was used, competition then does not promote stability. For saturating functional response we find, instead, that stability is increased for higher values of the co-operation parameter μ .

VIII. CONCLUSIONS

In summary we have analysed Lotka-Volterra communities with random interactions and non-linear functional response. Specifically, we have studied systems in which the total feedback on the growth rate of any one species saturates via a Holling type-II function. Simulations of such systems reveal three different types of behaviour. When the variation in interaction coefficients is small, convergence to stable fixed points is found for a wide range of values of the remaining model parameters. These fixed points are found to be unique, in the sense that the asymptotic composition of resulting community does not depend on the starting point of the dynamics for any realisation of the random interaction matrix. This stable behaviour is found provided the heterogeneity of interactions σ does not exceed a critical value. This critical value in turn depends on the combination of the parameter a indicating how steeply the feedback saturates, the co-operation parameter μ , and the symmetry parameter γ . Above the critical interaction strength two types of behaviours are found: when the heterogeneity in interaction coefficients is such that it promotes symmetric interactions we find that the LV dynamics has multiple stable fixed points, and which one is reached asymptotically depends on the choice of initial conditions. For negatively correlated heterogeneity instead we observe that the dynamics never settles down; volatile and potentially chaotic behaviour is seen.

The critical value for σ is much higher for a lower value for γ , with $\sigma_c \rightarrow \infty$ for $\gamma = -1$, when all interactions are exploitative. Low values of the saturation parameter (i.e., strongly non-linear feedback) increases the critical σ , i.e., the range of stability is larger. This effect is seen in particular when the cut-off a is smaller than the carrying capacity. Previous studies have found that stability decreases with an increasing co-operation parameter μ [6, 21, 22] in models with linear functional response. In this linear case the interaction with other species is not bounded, and a high degree of cooperation can lead to unlimited growth. With Holling type-II functional response the growth of abundances is bounded, and co-operation no longer prevents stable asymptotic fixed points. With nonlinear functional response we have found that increasing the co-operation parameter μ can increase stability, even when the functional response is linear over a wide range (i.e., when a is large); the key factor for stability is saturation at very large or very small arguments.

We conclude by briefly speculating about potential biological implications of our findings. The human gut has evolved with the microbiome, and has adapted to promote to stability as this is important for good health. Our findings suggest, that one effective way to increase the system's stability is to decrease γ , i.e., to exhibit more exploitative predator-prey like interactions. It may be difficult for the human gut to have an influence over the specific interactions types present between

the species, as these will be a function of the microbes themselves. The human gut has however, been found to promote ecosystem stability by host feeding, immune suppression and spatial structure [6] [7]. Spatial structure has the effect of reducing the interaction strength between populations of different species, which has the effect of reducing σ , which our model has shown to increase stability. Host feeding and immune suppression may work by enforcing a bound on species population size from above and below, which may result in a similar effect produced by nonlinear functional response explored in this paper. We have shown that enforcing a tight population bound (low a) promotes ecosystem stability, but also results in a higher system diversity (Fig. 3) which is also beneficial for health. Whilst employing nonlinear functional response, the cooperation within the system (parametrised by μ) can be increased without the adverse effect of destabilising the system [6]. This allows a more cooperative and efficient microbiome without compromising stability. Functional response has been observed in other ecosystems [44, 45, 48] and one would expect evolution to utilize this beneficial effect in the gut.

ACKNOWLEDGMENTS

We thank G. Biroli and F. Roy for discussions. LS acknowledges a PhD studentship by the Engineering and Physical Sciences Research Council (EPSRC UK), grant number EP/N509565/1. Partial financial support has been received from the Agencia Estatal de Investigacion (AEI, Spain) and Fondo Europeo de Desarrollo Regional (FEDER, EU) under Project PACSS (RTI2018-093732-B-C22), and the Maria de Maeztu Program for Units of Excellence in R&D (MDM-2017-0711).

Ecological communities from random Lotka-Volterra dynamics with nonlinear functional response

Laura Sidhom and Tobias Galla

— Supplementary Material —

S1. DETAILS OF THE GENERATING-FUNCTIONAL ANALYSIS

A. Expression for the generating functional

The Lotka-Volterra equations can be written as

$$\frac{\dot{x}_i(t)}{x_i(t)} = 1 - x_i(t) + g \left(\sum_j \alpha_{ij} x_j(t) + h_i(t) \right), \quad (\text{S1})$$

where we have introduced $h_i(t)$ to generate response functions and will be later set to zero.

We use this expression to set up the generating functional for the process,

$$\begin{aligned} Z[\boldsymbol{\psi}] = & \int D[\mathbf{x}] \exp \left(i \sum_i \int \psi_i(t) x_i(t) dt \right) \left[\prod_i p(x_i(0)) \right] \\ & \times \prod_{i,t} \delta \left\{ \frac{\dot{x}_i(t)}{x_i(t)} - \left[1 - x_i(t) + g \left(\sum_j \alpha_{ij} x_j(t) + h_i(t) \right) \right] \right\}, \end{aligned} \quad (\text{S2})$$

The integral $\int D[\mathbf{x}] = \prod_i \prod_t \int dx_i(t)$ is over all possible paths and random initial conditions; we assume that the latter factorise over the different species, i .

We can write the delta function as a Fourier transform to give

$$\begin{aligned} Z[\boldsymbol{\psi}] = & \int D\hat{\mathbf{x}} D\mathbf{x} \left[\prod_i p(x_i(0)) \right] \exp \left(i \sum_i \int \psi_i(t) x_i(t) dt \right) \\ & \times \exp \left\{ i \int \sum_i \hat{x}_i(t) \left[\frac{\dot{x}_i(t)}{x_i(t)} - 1 + x_i(t) - g \left(\sum_j \alpha_{ij} x_j(t) + h_i(t) \right) \right] dt \right\}, \end{aligned} \quad (\text{S3})$$

where factors of 2π have been absorbed in the measure via the definition

$$D\hat{\mathbf{x}} D\mathbf{x} \equiv \prod_i \prod_t \frac{d\hat{x}_i(t) dx_i(t)}{2\pi} \quad (\text{S4})$$

B. Auxiliary variable for disordered argument inside the functional response

In order to be able to carry out the disorder average at a later point, we isolate the terms containing the random coupling matrix by introducing the auxiliary variables

$$f_i(t) = \sum_j \alpha_{ij} x_j(t) + h_i(t). \quad (\text{S5})$$

In practical terms we do this by writing unity in the following form,

$$\int \delta[f_i(t) - \sum_j \alpha_{ij} x_j(t) - h_i(t)] df_i(t) = 1, \quad (\text{S6})$$

for all i and t . We then have

$$\int D\hat{\mathbf{f}} D\mathbf{f} \exp \left[i \sum_i \int \hat{f}_i(t) \left(f_i(t) - \sum_j \alpha_{ij} x_j(t) - h_i(t) \right) dt \right] = 1. \quad (\text{S7})$$

Inserting this into the generating functional, we find

$$\begin{aligned} Z[\psi] &= \int p(\mathbf{x}(0)) \exp \left(i \sum_i \int \psi_i(t) x_i(t) dt \right) \exp \left[i \int \sum_i \hat{x}_i(t) \left(\frac{\dot{x}_i(t)}{x_i(t)} - 1 + x_i(t) - g(f_i(t)) \right) dt \right] \\ &\times \exp \left[i \int \sum_i \hat{f}_i(t) \left(f_i(t) - \sum_j \alpha_{ij} x_j(t) - h_i(t) \right) dt \right] D\mathbf{f} D\hat{\mathbf{f}} D\mathbf{x} D\hat{\mathbf{x}}. \end{aligned} \quad (\text{S8})$$

For later purposes we introduce the average

$$\begin{aligned} &\langle F(\mathbf{f}, \hat{\mathbf{f}}, \mathbf{x}, \hat{\mathbf{x}}) \rangle \\ &= \int p(\mathbf{x}(0)) \exp \left[i \int \sum_i \hat{x}_i(t) \left(\frac{\dot{x}_i(t)}{x_i(t)} - 1 + x_i(t) - g(f_i(t)) \right) dt \right] \\ &\times \exp \left[i \int \sum_i \hat{f}_i(t) \left(f_i(t) - \sum_j \alpha_{ij} x_j(t) - h_i(t) \right) dt \right] F(\mathbf{f}, \hat{\mathbf{f}}, \mathbf{x}, \hat{\mathbf{x}}) D\mathbf{f} D\hat{\mathbf{f}} D\mathbf{x} D\hat{\mathbf{x}}, \end{aligned} \quad (\text{S9})$$

for functions (or functionals) $F(\mathbf{f}, \hat{\mathbf{f}}, \mathbf{x}, \hat{\mathbf{x}})$.

C. Calculation of moments from the generating functional

Moments of the dynamical variables are obtained as derivatives of the generating functional. For example, we have

$$\left. \frac{\partial Z[\psi]}{\partial \psi_i(t)} \right|_{\psi=0} = i \langle x_i(t) \rangle, \quad (\text{S10})$$

as well as

$$\left. \frac{\partial^2 Z[\psi]}{\partial \psi_i(t) \partial \psi_i(t')} \right|_{\psi=0} = -\langle x_i(t) x_i(t') \rangle. \quad (\text{S11})$$

Response functions can be obtained as follows,

$$\left. \frac{\partial^2 Z[\psi]}{\partial \psi_i(t) \partial h_i(t')} \right|_{\psi=0} = \frac{\partial \langle x_i(t) \rangle}{\partial h_i(t')} = \langle x_i(t) \hat{f}_i(t') \rangle. \quad (\text{S12})$$

It is also useful to note that $Z[\psi = \mathbf{0}] = 1$ for all choices of the perturbation fields $\{h_i(t)\}$. This indicates that

$$\frac{\partial Z[\psi = \mathbf{0}]}{\partial h_i(t)} = -i \langle \hat{f}_i(t) \rangle = 0, \quad (\text{S13})$$

and

$$\frac{\partial^2 Z[\psi = \mathbf{0}]}{\partial h_i(t) \partial h_i(t')} = -\langle \hat{f}_i(t) \hat{f}_i(t') \rangle = 0. \quad (\text{S14})$$

D. Disorder average

We now carry out the average over the disorder. The Gaussian random matrix elements α_{ij} have moments

$$\overline{\alpha_{ij}} = \frac{\mu}{N}, \quad \overline{\alpha_{ij}^2} - \frac{\mu^2}{N^2} = \frac{\sigma^2}{N}, \quad \overline{\alpha_{ij} \alpha_{ji}} - \frac{\mu^2}{N^2} = \frac{\gamma \sigma^2}{N}. \quad (\text{S15})$$

Focusing on the term in the generating functional containing the disorder, as $\alpha_{ii} = 0 \quad \forall i$, we find

$$\begin{aligned} & \overline{\exp \left(-i \int \sum_{i \neq j} \hat{f}_i(t) \alpha_{ij} x_j(t) dt \right)} \\ &= \exp \left(-\mu N \int F(t) M(t) dt - \frac{\sigma^2 N}{2} \int \{L(t, t') C(t, t') + \gamma K(t, t') K(t', t)\} dt dt' \right), \end{aligned} \quad (\text{S16})$$

where we have introduced the macroscopic variables

$$\begin{aligned} C(t, t') &= \frac{1}{N} \sum_i x_i(t) x_i(t'), \\ L(t, t') &= \frac{1}{N} \sum_i \hat{f}_i(t) \hat{f}_i(t'), \\ K(t, t') &= \frac{1}{N} \sum_i x_i(t) \hat{f}_i(t'), \\ M(t) &= \frac{1}{N} \sum_i x_i(t), \\ F(t) &= \frac{i}{N} \sum_i \hat{f}_i(t). \end{aligned} \quad (\text{S17})$$

It is also useful to introduce

$$J(t) = \frac{i}{N} \sum_i \hat{f}_i(t) f_i(t). \quad (\text{S18})$$

Inserting suitable delta-functions in their exponential representation similar to Eq. (S7) into the generating functional, we find

$$\overline{Z[\psi]} = \int \exp [N (\Omega + \Phi + \Psi)] D\mathbf{C}D\hat{\mathbf{C}}D\mathbf{L}D\hat{\mathbf{L}}D\mathbf{K}D\hat{\mathbf{K}}D\mathbf{M}D\hat{\mathbf{M}}D\mathbf{F}D\hat{\mathbf{F}}D\mathbf{J}D\hat{\mathbf{J}}, \quad (\text{S19})$$

with

$$\begin{aligned} \Omega = & \frac{1}{N} \sum_i \ln \left\{ \int p(x_i(0)) \exp \left(i \int \psi_i(t) x_i(t) dt \right) \exp \left(-i \int \hat{f}_i(t) h_i(t) dt \right) \right. \\ & \times \exp \left[i \int \hat{x}_i(t) \left(\frac{\dot{x}_i(t)}{x_i(t)} - 1 + x_i(t) - g(f_i(t)) \right) dt \right] \\ & \times \exp \left(-i \int \{ \hat{C}(t, t') x_i(t) x_i(t') + \hat{L}(t, t') \hat{f}_i(t) \hat{f}_i(t') + \hat{K}(t, t') x_i(t) \hat{f}_i(t') \} dt dt' \right) \\ & \left. \times \exp \left(-i \int \{ \hat{M}(t) x_i(t) + \hat{F}(t) i \hat{f}_i(t) + \hat{J}(t) i \hat{f}_i(t) f_i(t) \} dt \right) Df_i D\hat{f}_i D\hat{x}_i Dx_i \right\}, \end{aligned} \quad (\text{S20})$$

as well as

$$\begin{aligned} \Phi = & \int J(t) dt - \mu \int F(t) M(t) dt \\ & - \frac{\sigma^2}{2} \int \{ L(t, t') C(t, t') + \gamma K(t', t) K(t, t') \} dt dt', \end{aligned} \quad (\text{S21})$$

and

$$\begin{aligned} \Psi = & i \int \{ \hat{C}(t, t') C(t, t') + \hat{L}(t, t') L(t, t') + \hat{K}(t, t') K(t, t') \} dt dt' \\ & + i \int \{ \hat{M}(t) M(t) + \hat{F}(t) F(t) + \hat{J}(t) J(t) \} dt. \end{aligned} \quad (\text{S22})$$

The expression in Ω describes the time evolution of paths; this will be discussed further below. The term Φ results from the disorder average, and Ψ originates from the introduction of macroscopic order parameters.

E. Saddle-point integration

In the limit of $N \rightarrow \infty$, we can evaluate the integral in Eq. (S19) using the saddle-point approximation. To do this, we find the values of the dynamical order parameters at which the exponent in the integral becomes extremal.

Carrying out this extremisation, we find

$$\frac{\partial \Phi}{\partial C(t, t')} + \frac{\partial \Psi}{\partial C(t, t')} = 0 \implies i\hat{C}(t, t') = \frac{\sigma^2}{2} L(t, t'), \quad (\text{S23})$$

$$\frac{\partial \Phi}{\partial K(t, t')} + \frac{\partial \Psi}{\partial K(t, t')} = 0 \implies i\hat{K}(t, t') = \gamma \sigma^2 K(t', t), \quad (\text{S24})$$

$$\frac{\partial \Phi}{\partial L(t, t')} + \frac{\partial \Psi}{\partial L(t, t')} = 0 \implies i\hat{L}(t, t') = \frac{\sigma^2}{2} C(t, t'), \quad (\text{S25})$$

$$\frac{\partial \Phi}{\partial M(t)} + \frac{\partial \Psi}{\partial M(t)} = 0 \implies i\hat{M}(t) = \mu F(t), \quad (\text{S26})$$

$$\frac{\partial \Phi}{\partial F(t)} + \frac{\partial \Psi}{\partial F(t)} = 0 \implies i\hat{F}(t) = \mu M(t), \quad (\text{S27})$$

$$\frac{\partial \Phi}{\partial J(t)} + \frac{\partial \Psi}{\partial J(t)} = 0 \implies i\hat{J}(t) = -1. \quad (\text{S28})$$

$$\frac{\partial \Omega}{\partial \hat{C}(t, t')} + \frac{\partial \Psi}{\partial \hat{C}(t, t')} = 0 \implies C(t, t') = \lim_{N \rightarrow \infty} \frac{1}{N} \sum_i \langle x_i(t) x_i(t') \rangle_\Omega, \quad (\text{S29})$$

$$\frac{\partial \Omega}{\partial \hat{K}(t, t')} + \frac{\partial \Psi}{\partial \hat{K}(t, t')} = 0 \implies K(t, t') = \lim_{N \rightarrow \infty} \frac{1}{N} \sum_i \langle x_i(t) \hat{f}_i(t') \rangle_\Omega, \quad (\text{S30})$$

$$\frac{\partial \Omega}{\partial \hat{L}(t, t')} + \frac{\partial \Psi}{\partial \hat{L}(t, t')} = 0 \implies L(t, t') = \lim_{N \rightarrow \infty} \frac{1}{N} \sum_i \langle \hat{f}_i(t) \hat{f}_i(t') \rangle_\Omega, \quad (\text{S31})$$

$$\frac{\partial \Omega}{\partial \hat{M}(t)} + \frac{\partial \Psi}{\partial \hat{M}(t)} = 0 \implies M(t) = \lim_{N \rightarrow \infty} \frac{1}{N} \sum_i \langle x_i(t) \rangle_\Omega, \quad (\text{S32})$$

$$\frac{\partial \Omega}{\partial \hat{F}(t)} + \frac{\partial \Psi}{\partial \hat{F}(t)} = 0 \implies F(t) = \lim_{N \rightarrow \infty} \frac{i}{N} \sum_i \langle \hat{f}_i(t) \rangle_\Omega, \quad (\text{S33})$$

$$\frac{\partial \Omega}{\partial \hat{J}(t)} + \frac{\partial \Psi}{\partial \hat{J}(t)} = 0 \implies J(t) = \lim_{N \rightarrow \infty} \frac{i}{N} \sum_i \langle \hat{f}_i(t) f_i(t) \rangle_\Omega. \quad (\text{S34})$$

In these expressions we have introduced the notation

$$\langle A \rangle_\Omega = \frac{\int p(x(0)) A \exp(\omega) Df D\hat{f} D\hat{x} Dx}{\int p(x(0)) \exp(\omega) Df D\hat{f} D\hat{x} Dx}, \quad (\text{S35})$$

where

$$\begin{aligned}\omega = & i \int \psi(t)x(t)dt + i \int \hat{x}(t) \left(\frac{\dot{x}(t)}{x(t)} - 1 + x(t) - g(f(t)) \right) dt - i \int \hat{f}(t)h(t)dt \\ & - i \int \{ \hat{C}(t,t')x(t)x(t') + \hat{L}(t,t')\hat{f}(t)\hat{f}(t') + \hat{K}(t,t')x(t)\hat{f}(t') \} dt dt' \\ & - i \int \{ \hat{M}(t)x(t) + \hat{F}(t)i\hat{f}(t) + \hat{J}(t)i\hat{f}(t)f(t) \} dt\end{aligned}\quad (\text{S36})$$

is the argument of the exponential in Ω [Eq. (S20)],

$$\Omega = \ln \left[\int p(x(0)) \exp(\omega) Df D\hat{f} D\hat{x} Dx \right]. \quad (\text{S37})$$

We have assumed that $h_i(t) = h(t)$ and $p(x_i(0)) = p(x(0)) \forall i$, we find that the terms in the sum in Eq. (S20) are all identical, allowing us to drop the subscripts.

F. Further simplification

By differentiating this expression for the generating functional, taking the limit of $N \rightarrow \infty$, and comparing with Eqs. (S10)-(S14), we get

$$\overline{\langle x_i(t) \rangle} = -i \left. \frac{\partial \overline{Z[\boldsymbol{\psi}]}}{\partial \psi_i(t)} \right|_{\boldsymbol{\psi}=\mathbf{0}} = \langle x_i(t) \rangle_{\Omega[\boldsymbol{\psi}=\mathbf{0}]} \implies M(t) = -i \lim_{N \rightarrow \infty} \frac{1}{N} \sum_i \left. \frac{\partial \overline{Z[\boldsymbol{\psi}]}}{\partial \psi_i(t)} \right|_{\boldsymbol{\psi}=\mathbf{0}}, \quad (\text{S38})$$

$$\overline{\langle x_i(t)x_i(t') \rangle} = - \left. \frac{\partial^2 \overline{Z[\boldsymbol{\psi}]}}{\partial \psi_i(t) \partial \psi_i(t')} \right|_{\boldsymbol{\psi}=\mathbf{0}} = \langle x_i(t)x_i(t') \rangle_{\Omega[\boldsymbol{\psi}=\mathbf{0}]} \implies C(t,t') = - \lim_{N \rightarrow \infty} \frac{1}{N} \sum_i \left. \frac{\partial^2 \overline{Z[\boldsymbol{\psi}]}}{\partial \psi_i(t) \partial \psi_i(t')} \right|_{\boldsymbol{\psi}=\mathbf{0}}, \quad (\text{S39})$$

$$\left. \frac{\partial \overline{\langle x_i(t) \rangle}}{\partial h_i(t')} \right|_{\boldsymbol{\psi}=\mathbf{0}} = -i \left. \frac{\partial^2 \overline{Z[\boldsymbol{\psi}]}}{\partial \psi_i(t) \partial h_i(t')} \right|_{\boldsymbol{\psi}=\mathbf{0}} = -i \langle x_i(t) \hat{f}_i(t') \rangle_{\Omega[\boldsymbol{\psi}=\mathbf{0}]} \implies K(t,t') = \lim_{N \rightarrow \infty} \frac{1}{N} \sum_i \left. \frac{\partial^2 \overline{Z[\boldsymbol{\psi}]}}{\partial \psi_i(t) \partial h_i(t')} \right|_{\boldsymbol{\psi}=\mathbf{0}}, \quad (\text{S40})$$

$$\left. \frac{\partial \overline{Z[\boldsymbol{\psi}=\mathbf{0}]}}{\partial h_i(t)} \right|_{\boldsymbol{\psi}=\mathbf{0}} = -i \langle \hat{f}_i(t) \rangle_{\Omega[\boldsymbol{\psi}=\mathbf{0}]} = 0 \implies F(t) = 0, \quad (\text{S41})$$

$$\left. \frac{\partial^2 \overline{Z[\boldsymbol{\psi}=\mathbf{0}]}}{\partial h_i(t) \partial h_i(t')} \right|_{\boldsymbol{\psi}=\mathbf{0}} = - \langle \hat{f}_i(t) \hat{f}_i(t') \rangle_{\Omega[\boldsymbol{\psi}=\mathbf{0}]} = 0 \implies L(t,t') = 0. \quad (\text{S42})$$

These equations demonstrate that taking the average over the random matrix elements in the limit $N \rightarrow \infty$ gives the same result as taking the average with respect to Ω as described above in Eq. (S35), and setting $\boldsymbol{\psi} = \mathbf{0}$. This average gives a generating functional for a dynamics of an effective process for a single species; we will discuss this next.

G. Effective single-species process

We insert our results from the saddle point method, Eqs. (S23) to (S28), and find

$$\langle A[x] \rangle_{\Omega[\psi=0]} = \frac{\int A[x] P[x] Dx}{\int P[x] Dx}, n \quad (\text{S43})$$

where

$$\begin{aligned} P[x] = & p(x(0)) \exp \left(-i \int \hat{f}(t) h(t) dt \right) \exp \left[i \int \hat{x}(t) \left(\frac{\dot{x}(t)}{x(t)} - 1 + x(t) - g(f(t)) \right) dt \right] \\ & \times \exp \left(- \int \left\{ \frac{\sigma^2}{2} C(t, t') \hat{f}(t) \hat{f}(t') + \gamma \sigma^2 K(t', t) x(t) \hat{f}(t') \right\} dt dt' \right) \\ & \times \exp \left(-i \int \{ \mu M(t) \hat{f}(t) - \hat{f}(t) f(t) \} dt \right) Df D\hat{f} D\hat{x}. \end{aligned} \quad (\text{S44})$$

This is the probability of observing a path of the effective process given by the evolution equation

$$\dot{x}(t) = x(t) \left[1 - x(t) + g \left(\mu M(t) + \gamma \sigma^2 \int_0^t G(t, t') x(t') dt' + h(t) + \eta(t) \right) \right], \quad (\text{S45})$$

where

$$M(t) = \langle x(t) \rangle_*, \quad (\text{S46})$$

$$\langle \eta(t) \eta(t') \rangle_* = \sigma^2 C(t, t') = \sigma^2 \langle x(t) x(t') \rangle_*, \quad (\text{S47})$$

$$G(t, t') = -i K(t, t') = \left\langle \frac{\partial x(t)_*}{\partial h(t')} \right\rangle, \quad (\text{S48})$$

where $\langle \dots \rangle_*$ is the average over the effective process. The statistics of realisations of this effective process are the same as those of the individual species trajectories in the original model. Hence we can use the effective process to find fixed points of the original system, and analyse their stability.

H. Fixed-point analysis

We now assume the system reaches a stable unique fixed point, $x(t) \rightarrow x^*$, which does not depend on initial conditions. This means that the macroscopic order parameters will tend to a constant, $M(t) \rightarrow M^*$ and $C(t + \tau, t) \rightarrow q \forall \tau$ as $t \rightarrow \infty$. At a fixed point the response function becomes time-translation invariant, $G(t, t') = G(t - t')$, and a perturbation from a stable fixed point will have no long term effects; the integrated response function remains finite, $\chi = \int_0^\infty G(\tau) d\tau < \infty$ (see. e.g. [17]). Each realization of $\eta(t)$ tends to a static Gaussian random variable η^* at large times, with $\langle \eta^* \rangle = 0$ and $\langle \eta^{*2} \rangle = \sigma^2 q$. We can then write η as $\sigma \sqrt{q} z$ where z is a standard Gaussian random number. We can now set $h(t)$ to zero, and instead generate response functions from $\eta(t)$ via

$$G(t, t') = \left\langle \frac{\partial x(t)}{\partial \eta(t')} \right\rangle_*. \quad (\text{S49})$$

Fixed points satisfy the condition

$$x^* [1 - x^* + g(\mu M^* + \gamma \sigma^2 \chi x^* + \sigma \sqrt{q} z)] = 0. \quad (\text{S50})$$

For any value of z , this relation has the solution $x^*(z) = 0$. Other solutions can be found from

$$g(\mu M^* + \gamma \sigma^2 \chi x^* + \sigma \sqrt{q} z) = x^* - 1, \quad (\text{S51})$$

and are only valid if they are non-negative (x^* represents the abundance of the effective species). We now evaluate this for the clipped functional response defined by

$$g(u) = g_P(u) = \begin{cases} a & u \geq a \\ u & -a \leq u \leq a \\ -a & u \leq -a. \end{cases} \quad (\text{S52})$$

The function consists of three segments, we look at each of these individually.

- (i) If $\mu M^* + \gamma \sigma^2 \chi x^* + \sigma \sqrt{q} z \geq a$ we have, $g = a$, and hence $a = x^* - 1$ from Eq. (S51). Substituting $x^* = a + 1$ into the argument of g leads to the condition

$$\mu M^* + \gamma \sigma^2 \chi(a + 1) + \sigma \sqrt{q} z \geq a \quad (\text{S53})$$

this implies

$$z \geq \frac{(a + 1)(1 - \gamma \sigma^2 \chi) - (\mu M^* + 1)}{\sigma \sqrt{q}}. \quad (\text{S54})$$

For later convenience we introduce the short-hand

$$z_2 \equiv \frac{(a + 1)(1 - \gamma \sigma^2 \chi) - (\mu M^* + 1)}{\sigma \sqrt{q}}. \quad (\text{S55})$$

- (ii) saturated at lower end [$g(u) = -a$] For the case $\mu M^* + \gamma \sigma^2 \chi x^* + \sigma \sqrt{q} z \leq -a$, we have $g = -a$ and $x^* = 1 - a$. As x^* cannot be negative, we substitute $x^* = (1 - a)\Theta(1 - a)$ into the argument of g to find

$$\mu M^* + \gamma \sigma^2 \chi(1 - a)\Theta(1 - a) + \sigma \sqrt{q} z \leq -a \quad (\text{S56})$$

this implies

$$z \leq \begin{cases} \frac{-a - \mu M^*}{\sigma \sqrt{q}} & a \geq 1, \\ \frac{(1 - a)(1 - \gamma \sigma^2 \chi) - (1 + \mu M^*)}{\sigma \sqrt{q}} & a \leq 1. \end{cases} \quad (\text{S57})$$

- (iii) If $-a \leq (\mu M^* + \gamma \sigma^2 \chi x^* + \sigma \sqrt{q} z) \leq a$, we have $(\mu M^* + \gamma \sigma^2 \chi x^* + \sigma \sqrt{q} z) = x^* - 1$ from Eq. (S51). This gives

$$x^* = \frac{1 + \mu M^* + \sigma \sqrt{q} z}{1 - \gamma \sigma^2 \chi} \Theta \left(\frac{1 + \mu M^* + \sigma \sqrt{q} z}{1 - \gamma \sigma^2 \chi} \right), \quad (\text{S58})$$

where the Heaviside function again ensures that the solution is non-negative. Substituting this into $-a \leq (\mu M^* + \gamma \sigma^2 \chi x^* + \sigma \sqrt{q} z) \leq a$, we find

$$-a \leq \mu M^* + \gamma \sigma^2 \chi \frac{1 + \mu M^* + \sigma \sqrt{q} z}{1 - \gamma \sigma^2 \chi} \Theta \left(\frac{1 + \mu M^* + \sigma \sqrt{q} z}{1 - \gamma \sigma^2 \chi} \right) + \sigma \sqrt{q} z \leq a \quad (\text{S59})$$

We can take the two possible values of the Heaviside function in turn and rearrange Eq. (S59) into conditions for z .

- (a) For a negative argument of the Heaviside function we have

$$x^* = 0 \quad \text{for} \quad \frac{-a - \mu M^*}{\sigma \sqrt{q}} \leq z \leq \frac{-1 - \mu M^*}{\sigma \sqrt{q}}. \quad (\text{S60})$$

We note that for this case to occur we require the upper limit for z in Eq. (S60) to be greater than the lower limit, requiring $a \geq 1$.

We have now found two intervals for z where $x^* = 0$ for $a \geq 1$: one in Eq. (S57) and another in Eq. (S60). Combining these, we find

$$x^* = 0 \quad \text{for} \quad z \leq \frac{-1 - \mu M^*}{\sigma \sqrt{q}} \quad \text{for} \quad a \geq 1. \quad (\text{S61})$$

- (b) For a positive argument in the Heaviside function we find

$$x^* = \frac{1 + \mu M^* + \sigma \sqrt{q} z}{1 - \gamma \sigma^2 \chi}, \quad (\text{S62})$$

this applies when

$$\frac{(1 - a)(1 - \gamma \sigma^2 \chi) \Theta(1 - a) - (\mu M^* + 1)}{\sigma \sqrt{q}} \leq z \leq \frac{(1 + a)(1 - \gamma \sigma^2 \chi) - (\mu M^* + 1)}{\sigma \sqrt{q}}. \quad (\text{S63})$$

Putting these three branches for g together we find

$$x^* = \begin{cases} a + 1 & z \geq z_2 \\ \frac{1 + \mu M^* + \sigma \sqrt{q} z}{1 - \gamma \sigma^2 \chi} & z_1 \leq z \leq z_2 \\ (1 - a) \Theta(1 - a) & z \leq z_1, \end{cases} \quad (\text{S64})$$

where z_2 is as given in Eq. (S55) and

$$z_1 \equiv \frac{(1 - a)(1 - \gamma \sigma^2 \chi) \Theta(1 - a) - (1 + \mu M^*)}{\sigma \sqrt{q}}. \quad (\text{S65})$$

We can then simplify and solve the self-consistency relations in Eqs. (13a,13b,13c) to find the values of these parameters for fixed points. Writing $Dz = \frac{e^{-z^2/2}}{\sqrt{2\pi}} dz$ find

$$M^* = \int_{z_2}^{\infty} (a+1) Dz + \int_{z_1}^{z_2} \frac{1 + \mu M^* + \sigma \sqrt{q} z}{1 - \gamma \sigma^2 \chi} Dz + \int_{-\infty}^{z_1} (1-a) \Theta(1-a) Dz \quad (\text{S66})$$

for the biomass at the fixed point, as well as

$$q = \int_{z_2}^{\infty} (a+1)^2 Dz + \int_{z_1}^{z_2} \left(\frac{1 + \mu M^* + \sigma \sqrt{q} z}{1 - \gamma \sigma^2 \chi} \right)^2 Dz + \int_{-\infty}^{z_1} (1-a)^2 \Theta(1-a) Dz \quad (\text{S67})$$

for the second moment of species abundances ($q = \langle x^2 \rangle_*$). The integrated response is obtained as

$$\begin{aligned} \chi &= \int_0^{\infty} G(\tau) d\tau \\ &= \int_0^{\infty} \left\langle \frac{\partial x(t)}{\partial \eta(t-\tau)} \right\rangle d\tau \\ &= \left\langle \frac{\partial x(\eta^*)}{\partial \eta^*} \right\rangle \\ &= \int_{z_1}^{z_2} \frac{1}{1 - \gamma \sigma^2 \chi} Dz. \end{aligned} \quad (\text{S68})$$

It is also useful to introduce $\phi = \int_{z_1}^{z_2} Dz$ as the probability of the abundance of the effective species not saturating [neither at $x^* = 1+a$ nor at $x^* = (1-a)\Theta(1-a)$]. This quantity describes the fraction of species that do not saturate in the original dynamics.

Using Eq. (S68) we have

$$\phi = \chi(1 - \gamma \sigma^2 \chi). \quad (\text{S69})$$

I. Linear stability analysis

We consider a small perturbation from the fixed point, and find the conditions for instability. The expressions for the macroscopic order parameters χ , ϕ , M^* and q in the previous section are based on the assumption of a unique stable fixed point; hence they are only valid for model parameters in which such a unique fixed point exists, and is stable. To carry out the linear stability analysis, we start from the effective process

$$\dot{x}(t) = x(t) \left[1 - x(t) + g \left(\mu M(t) + \gamma \sigma^2 \int_0^t G(t, t') x(t') dt' + \eta(t) \right) \right]. \quad (\text{S70})$$

We follow the steps of [17] and write $x(t) = x^* + y(t)$ and $\eta(t) = \sigma \sqrt{q} z + v(t)$ with $\langle y(t) \rangle = \langle v(t) \rangle = 0$. We note that the order parameter M experiences no contribution from the perturbation $y(t)$, as the ansatz assumes zero-average fluctuations about the fixed points. Self-consistency further requires $\langle v(t)v(t') \rangle = \sigma^2 \langle y(t)y(t') \rangle$.

Substituting this ansatz into the effective process leads to

$$\dot{y}(t) = (x^* + y(t)) \left[1 - x^* - y(t) + g \left(\mu M^* + \gamma \sigma^2 \int_0^t G(t, t') (x^* + y(t')) dt' + \sigma \sqrt{q} z + v(t) \right) \right]. \quad (\text{S71})$$

We investigate the stability of the two fixed points separately:

- (i) First we investigate the fixed point $x^*(z) = 0$. We then have

$$\dot{y}(t) = y(t) \left[1 - y(t) + g \left(\mu M^* + \gamma \sigma^2 \int_0^t G(t, t') y(t') dt' + \sigma \sqrt{q} z + v(t) \right) \right], \quad (\text{S72})$$

which we linearise to obtain

$$\dot{y}(t) = [1 + g(\mu M^* + \sigma \sqrt{q} z)] y(t). \quad (\text{S73})$$

We now distinguish several cases:

- (a) For $z \geq (a - \mu M^*)/(\sigma \sqrt{q})$, we have $g(u) = a$, we find $\dot{y}(t) = (1 + a)y(t)$. Hence $x^* = 0$ is unstable.
- (b) For $z \leq (-a - \mu M^*)/(\sigma \sqrt{q})$, we have $g(u) = -a$, and we find $\dot{y}(t) = (1 - a)y(t)$. The zero fixed point is stable when $a \geq 1$.
- (c) For $(-a - \mu M^*)/(\sigma \sqrt{q}) \leq z \leq (a - \mu M^*)/(\sigma \sqrt{q})$ we have $g(u) = u$, we find $\dot{y}(t) = (1 + \mu M^* + \sigma \sqrt{q} z)y(t)$. Hence, the zero fixed point is stable if $z \leq -(1 + \mu M^*)/(\sigma \sqrt{q})$. Therefore we require $-a - \mu M^* \leq -1 - \mu M^*$ for stable fixed points of this type to exist, i.e., $a \geq 1$.

We note that $x^* = 0$ is stable only for the cases where it is the unique fixed point, which is when $z \leq z_1$ and $a \geq 1$, these conditions were met for stability in cases (ii) and (iii).

- (ii) Now we consider the stability of the other fixed points found in the previous section. These satisfy

$$1 - x^* + g \left(\mu M^* + x^* \gamma \sigma^2 \int_0^t G(t, t') dt' + \sigma \sqrt{q} z \right) = 0. \quad (\text{S74})$$

For $z \geq z_2$ or $z \leq z_1$, the functional is saturated, $|g(u)| = a$, and a slight perturbation will not change the value of the function, $g(u + du) = g(u)$. This gives $\dot{y}(t) = -y(t)x^*$ from Eq. (S71) to linear order. Hence the fixed point is stable.

To determine stability of the fixed in the case $z_1 \leq z \leq z_2$, we have $g(u) = u$, we follow [17] and add a noise variable $\xi(t)$ with $\langle \xi(t) \rangle = 0$, and which we can take to be of unit amplitude.

We then have

$$\dot{y}(t) = (x^* + y(t)) \left(1 - x^* - y(t) + \mu M^* + \gamma \sigma^2 \int_0^t G(t, t') (x^* + y(t')) dt' + \sigma \sqrt{q} z + v(t) + \xi(t) \right). \quad (\text{S75})$$

Linearizing, we obtain

$$\dot{y}(t) = x^* \left(-y(t) + \gamma \sigma^2 \int_0^t G(t, t') y(t') dt' + v(t) + \xi(t) \right). \quad (\text{S76})$$

Carrying out a Fourier transform, we find

$$\frac{i\omega \tilde{y}(\omega)}{x^*} = (\gamma \sigma^2 \tilde{G}(\omega) - 1) \tilde{y}(\omega) + \tilde{v}(\omega) + \tilde{\xi}(\omega), \quad (\text{S77})$$

which rearranges to

$$\tilde{y}(\omega) = \frac{\tilde{v}(\omega) + \tilde{\xi}(\omega)}{\frac{i\omega}{x^*} + (1 - \gamma \sigma^2 \tilde{G}(\omega))}. \quad (\text{S78})$$

We focus on the case $\omega = 0$ (see also [29, 30]), noting that the integrated response is $\chi = \tilde{G}(0) = \int_0^\infty G(\tau) d\tau$. We find

$$\langle \tilde{y}(0) \tilde{y}^*(0) \rangle_{ns} = \frac{\langle \tilde{v}(0) \tilde{v}^*(0) \rangle_{ns} + \langle \tilde{\xi}(0) \tilde{\xi}^*(0) \rangle_{ns}}{(1 - \gamma \sigma^2 \chi)^2}, \quad (\text{S79})$$

where the subscript ‘ns’ indicates that the average is over species with non-saturated functional response only. As introduced above, these make up a fraction ϕ of all species at the fixed points. The remaining saturated species are stable and do not contribute to the statistics of perturbations.

Noting that $\langle v(t) v(t') \rangle = \sigma^2 \langle y(t) y(t') \rangle$, and hence $\langle \tilde{v}(0) \tilde{v}^*(0) \rangle = \sigma^2 \langle \tilde{y}(0) \tilde{y}^*(0) \rangle$, we find

$$\langle |\tilde{y}(0)|^2 \rangle = \frac{\phi(\sigma^2 \langle |\tilde{y}(0)|^2 \rangle + 1)}{(1 - \gamma \sigma^2 \chi)^2}. \quad (\text{S80})$$

The factor of ϕ accounts for the fact that the above analysis only applies to species for which the functional response is not saturated, and that all other species are stable (as indicated by the condition $z_1 \leq z \leq z_2$ in Sec. S1 I).

Re-arranging Eq. (S80) we have

$$\langle |\tilde{y}(0)|^2 \rangle = \frac{\phi}{(1 - \gamma \sigma^2 \chi)^2 - \phi \sigma^2}. \quad (\text{S81})$$

In order for the fixed points to be stable this quantity needs to be finite. By construction, it also must be non-negative. The stable phase is therefore characterised by $(1 - \gamma \sigma^2 \chi)^2 > \phi \sigma^2$,

and the onset of instability occurs when $(1 - \gamma\sigma^2\chi)^2 = \phi\sigma^2$. Using Eq. (S69) we find the following critical strength of the coupling matrix elements,

$$\sigma_c^2 = \frac{1}{\chi(1 + \gamma)}. \quad (\text{S82})$$

The susceptibility χ is to be obtained from the self-consistency equations (S66,S67,S68).

J. Minimum value for σ_c in Fig. 9

The minimum value of σ_c with respect to μ found in Fig. 9 corresponds to a maximum value of the proportion of unsaturated species ϕ . To show this, we begin with the instability condition in Eq. (S82), and differentiate with respect to μ (at fixed γ),

$$2\chi\sigma_c \frac{\partial\sigma_c}{\partial\mu} + \sigma_c^2 \frac{\partial\chi}{\partial\mu} = 0, \quad (\text{S83})$$

which results in $\frac{\partial\chi}{\partial\mu} = 0$ for $\frac{\partial\sigma_c}{\partial\mu} = 0$ and nonzero σ_c . By differentiating Eq. (13c) with respect to μ we find that $\frac{\partial\chi}{\partial\mu} = 0$ implies $\frac{\partial\phi}{\partial\mu} = 0$.

S2. NUMERICAL INTEGRATION OF THE LOTKA-VOLTERRA EQUATIONS

A. Interaction matrix and integration

For any pair $i < j$, the elements α_{ij} and α_{ji} in the interaction matrix are correlated (for $\gamma \neq 0$). To generate such matrices we proceed as follows: for each pair $i < j$ draw two independent Gaussian random numbers $r_1, r_2 \sim N(0, 1)$ and set $\alpha_{ij} = \frac{\mu}{N} + \frac{\sigma}{\sqrt{N}}r_1$ and $\alpha_{ji} = \frac{\mu}{N} + \frac{\sigma}{\sqrt{N}}(\gamma r_1 + \sqrt{1 - \gamma^2}r_2)$. This ensures the entries have the required mean μ/N , variance σ^2/N , and co-variance $\gamma\sigma^2/N$. We set the diagonal elements of the interaction matrix to zero, $\alpha_{ii} = 0$.

The Lotka-Volterra system is a system of N coupled ordinary differential equations. We typically choose N to be in the range 100-300. The system of ordinary differential equations is then integrated using a Runge-Kutta (RK4) integration scheme, with a time step $\Delta t = 0.001$.

B. Order parameters from numerical integration of the Lotka-Volterra equations

The data shown in Figs. (3,4,6,7) is from numerical integration of the system with $N = 200$. We initialise the system by drawing each $x_i(0)$ randomly from a uniform distribution on $[0, 1]$. The integration is then carried out up to a final time $T = 200$.

For each realisation, the macroscopic order parameters were calculated as $M = \frac{1}{N} \sum_i \langle x_i \rangle_t$, $q = \frac{1}{N} \sum_i \langle x_i^2 \rangle_t$, where $\langle \cdots \rangle_t$ denotes a time average in the stationary state; numerically this is carried out as the average over the last 1% of the trajectory. This was then subsequently averaged over 20 realisations of the random coupling matrix.

In order to characterise the dynamic behaviour of the system, we also calculate the variance of the trajectory $h = \frac{\langle \langle x_i(t)^2 \rangle_t - \langle x_i(t) \rangle_t^2 \rangle_N}{\langle \langle x_i(t) \rangle_t^2 \rangle_N}$, see also [31]. We use the notation $\langle x_i \rangle_N = N^{-1} \sum_i x_i$ to indicate averages over species in the numerical integration. In order to detect possible dependence on initial conditions (and convergence to multiple different fixed points from different initial conditions), we have also carried out numerical work in which we draw one fixed instance of the interaction matrix, and then start two copies of this system. Labelling the coordinates of the two copies as x_i and x'_i respectively, we then calculate $d = \left\langle \frac{\langle (x_i - x'_i)^2 \rangle_N}{\langle x_i \rangle_N^2} \right\rangle_t$. A non-zero value of this quantity at long times indicates that dependence on initial conditions.

Broadly speaking the case $h = 0, d = 0$ indicates that the system converges to a fixed point and that this fixed point is unique, in the sense that it does not depend on initial conditions. The case $h = 0, d > 0$ indicates that system converges, but that fixed point depends on initial condition (i.e., multiple stable fixed points exist). For $h > 0$ finally, the system does not converge to fixed points. We have not attempted to systematically characterise potential chaotic behaviour, or to distinguish it from limit-cycle dynamics.

C. Species abundance distributions

In Fig. S1 we present histograms similar to that in Fig. 2, but for a cut-off of the functional response at $a = 2$ instead of $a = 0.5$. For this case, a is above the carrying capacity; species then die out before they can reach the lower saturation point of $1 - a$. For this case we find the upper boundary $(1 + a)$ to be higher, and therefore a larger heterogeneity σ is required to spread the distribution enough for some species to reach upper saturation.

Each of the histograms in Figs. 2 and S1 was generated from 100 simulations with $N = 200$ run up to final time $T = 200$.

D. Phase diagrams

To plot the phase diagrams in the main paper (Figs. 1 and 5), we simulated the system for $N = 200$ for each value of γ and σ , up to final time $T = 200$. If, at any time during the simulation, any of the species abundances became greater than 10^5 , then simulation was stopped and the system

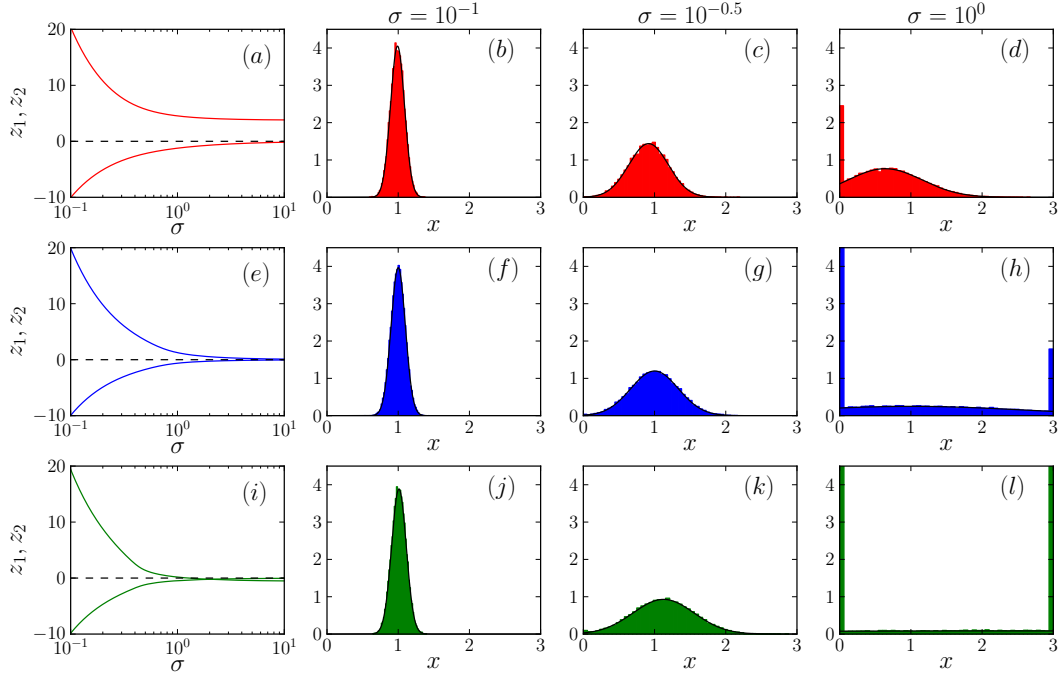


FIG. S1. Species abundance distribution for the case $a = 2$ and $\mu = 0$ for different values of the heterogeneity σ . The upper row [panels (a)-(d)] is for $\gamma = -1$, the middle row [(e)-(h)] for $\gamma = 0$, and the lower row [(i)-(l)] for $\gamma = 1$. On the left [(a),(e),(i)] we show z_2 (upper line) and z_1 (lower line), remaining panels show the species abundance distributions, for $\sigma = 10^{-1}$ [(b),(f),(j)], $\sigma = 10^{-0.5}$ [(c),(g), (k)] and $\sigma = 1$ [(d),(h),(l)]. Solid lines are theoretical predictions for the species abundance distribution, shaded histograms are from simulations.

was classified as divergent. If after the simulation had completed, no species abundance x_i changed by more than 0.0001 in any integration step during the last 1% of the run, $|x_i(t) - x_i(t-1)| < 0.0001 \quad \forall \quad 1 \leq i \leq N, \quad 0.99T \leq t \leq T$, then the system was classified as fixed. If this condition was not met then we carried out the following additional check for convergence: if the change in abundance for each species was constantly decreasing during the last 1% of the run, $|x_i(t) - x_i(t-1)| < |x_i(t-1) - x_i(t-2)|$ for all $1 \leq i \leq N$ and $0.99T \leq t \leq T$, then we assumed that it would converge to a fixed point, so was also classed as fixed.

If the system was found to converge to a fixed point then it was checked for uniqueness; this was done as follows. For each realisation of the interaction matrix, two trajectories were simulated with random initial conditions, $x_i(0), x'_i(0)$, drawn from the interval between 0 and 1 with uniform distribution. If $|x_i(t) - x'_i(t)| < 0.0001$ for all $1 \leq i \leq N$ and $0.99T \leq t \leq T$ then the fixed point was classified as unique. If this condition was not met then we carried out the following additional check: if the change in difference between each species abundance was constantly decreasing during the last 1% of the run, $|x_i(t) - x'_i(t)| < |x_i(t-1) - x'_i(t-1)|$ for all $1 \leq i \leq N$ and all $0.99T \leq t \leq T$, then

we assumed that they will converge to the same value, so the fixed point was classified as unique.

For each combination of model parameters 200 realisations of the interaction matrix were simulated, and had its behaviour classified. The behaviours observed were plotted as a colour with code [RGB] (red-green-blue): the red component represents the proportion of realizations that converged to a unique fixed point, the green component that of runs with multiple fixed points, and the blue component non convergent dynamics.

S3. NUMERICAL SOLUTION OF SELF-CONSISTENT EQUATIONS FOR MACROSCOPIC ORDER PARAMETERS

A. Finding fixed point values for given z_1 and z_2

The self consistency equations (13) cannot be solved directly for a given choice of model parameters σ, γ, a and μ . This is because one would first need to evaluate the quantities z_1 and z_2 , which are present on the right-hand side of Eqs. (13). At the same time, z_1 and z_2 are functions of the order parameters we wish to find, see Eqs. (11).

We therefore take a parametric approach. We can solve Eqs. (13) for the set of variables $\{M^*, \chi, q, \phi, \gamma, \sigma\}$ for given values of $\{z_1, z_2, a, \mu\}$. Using Eqs. (11), we first introduce new parameters p_1 and p_2 ,

$$\begin{aligned} p_1 &\equiv \frac{(1 - \gamma\sigma^2\chi)}{\sigma\sqrt{q}} = \frac{z_2 - z_1}{1 + a - (1 - a)\Theta(1 - a)}, \\ p_2 &\equiv \frac{1 + \mu M^*}{\sigma\sqrt{q}} = \frac{(1 - a)\Theta(1 - a)z_2 - (1 + a)z_1}{1 + a - (1 - a)\Theta(1 - a)}. \end{aligned} \quad (\text{S84})$$

These can be found for given z_1 and z_2 . Next, we can express the self-consistency relations in Eqs. (13) in terms of p_1 and p_2 , to find M^* , q and ϕ . We have

$$\begin{aligned} M^* &= \frac{1 + a}{2} \left[1 - \operatorname{erf} \left(\frac{z_2}{\sqrt{2}} \right) \right] + \frac{p_2}{2p_1} \left[\operatorname{erf} \left(\frac{z_2}{\sqrt{q}} \right) - \operatorname{erf} \left(\frac{z_1}{\sqrt{2}} \right) \right] \\ &+ \frac{1}{\sqrt{2\pi}p_1} \left[\exp \left(\frac{-z_1^2}{2} \right) - \exp \left(\frac{-z_2^2}{2} \right) \right] + \frac{(1 - a)\Theta(1 - a)}{2} \left[1 + \operatorname{erf} \left(\frac{z_1}{\sqrt{2}} \right) \right], \end{aligned} \quad (\text{S85})$$

as well as

$$\begin{aligned} q &= \frac{(1 + a)^2}{2} \left[1 - \operatorname{erf} \left(\frac{z_2}{\sqrt{2}} \right) \right] + \frac{p_2^2 + 1}{2p_1^2} \left[\operatorname{erf} \left(\frac{z_2}{\sqrt{2}} \right) - \operatorname{erf} \left(\frac{z_1}{\sqrt{2}} \right) \right] \\ &+ \frac{p_2}{\sqrt{2\pi}p_1^2} \left[\exp \left(\frac{-z_1^2}{2} \right) - \exp \left(\frac{-z_2^2}{2} \right) \right] - \frac{1 + a}{\sqrt{2\pi}p_1} \exp \left(\frac{-z_2^2}{2} \right) \\ &+ \frac{(1 - a)\Theta(1 - a)}{\sqrt{2\pi}p_1} \exp \left(\frac{-z_1^2}{2} \right) + \frac{(1 - a)^2\Theta(1 - a)}{2} \left[1 - \operatorname{erf} \left(\frac{z_1}{\sqrt{2}} \right) \right], \end{aligned} \quad (\text{S86})$$

and

$$\phi = \frac{1}{2} \left[\operatorname{erf} \left(\frac{z_2}{\sqrt{2}} \right) - \operatorname{erf} \left(\frac{z_1}{\sqrt{2}} \right) \right]. \quad (\text{S87})$$

Now that we have M^* and q , we can find σ via

$$\sigma = \frac{1 + \mu M^*}{p_2 \sqrt{q}}. \quad (\text{S88})$$

We define another new parameter $k \equiv 1 - \gamma \sigma^2 \chi$ which we evaluate using σ via

$$k \equiv 1 - \gamma \sigma^2 \chi = p_3 \sigma \sqrt{q}, \quad (\text{S89})$$

which can now be used to find χ and γ via

$$\chi = \frac{\phi}{2k}, \quad (\text{S90})$$

$$\gamma = \frac{1 - k}{\chi \sigma^2}. \quad (\text{S91})$$

In Fig. 3 we plot graphs for the quantities ϕ , M , as well as the diversity for varying values of σ while keeping the symmetry parameter γ fixed. The predictions for from the theory were extracted from Eqs. (13) as follows: Let the function $g(z_1, z_2, a, \mu)$ denote the value for γ that we obtain from the algorithm described in the previous section. For any particular value of z_2 there should be a unique value of z_1 such that $g(z_1, z_2, a, \mu) = \gamma_f$, where γ_f is the desired fixed value of the symmetry parameter. We can find this value for z_1 by finding the root of the function $G(z_1) = g(z_1, z_2, a, \mu) - \gamma_f$ using the Newton–Raphson method. To plot the lines in Figs. 3 and 7, we chose values of γ_f, a, μ , and varied z_2 to get a values of ϕ , M and diversity for a range of σ . The solutions were then parametrically plotted as a function of σ .

B. Numerical identification of the instability line for continuous a

To find the critical value of the interaction strenth, σ_c , for fixed parameters μ, a, γ shown in Fig. 8, we set fixed values for the parameters μ and a , and find values z_1 and z_2 resulting in the desired value of γ while satifsying Eq. (S82). In principle this can be done by scanning the two-dimensional plane spanned by z_1 and z_2 . Instead we used a two dimensional Newton-Raphson algorithm. This consisted of a Newton-Raphson on z_1 to find the correct γ inside a Newton-Raphson procedure for z_2 to satisfy Eq. (S82).

For the outer Newton-Raphson on z_2 , let the function $s(z_2, \gamma, a, \mu)$ denote the value for $\chi \sigma^2$ that we obtain from finding the corresponding z_1 for γ , at given z_2 . The critical value for σ fulfills

$\chi\sigma_c^2 = 1/(1 + \gamma)$, so instability occurs when $s(z_2, \gamma, a, \mu) = 1/(1 + \gamma)$. We found that $s(z_2, \gamma, a, \mu)$ contained a singularity, so instead we took the inverse of this function, and used Newton-Raphson to find the root of $S(z_2) = 1/s(z_2, \gamma, a, \mu) - (1 + \gamma)$.

For each value of z_2 that $S(z_2)$ was evaluated for during the algorithm, a corresponding value for z_1 had to be found to obtain the required γ . The solution for z_1 found for a value of z_2 was used as an initial value for find z_1 for the next value of z_2 in the Newton-Raphson algorithm.

C. Numerical identification of the instability line for different values of μ

We found that we were not able to use the algorithm described above to generate Fig. 9 as the function $G(z_1) = g(z_1, z_2, a, \mu) - \gamma_f$ was not well behaved for $\mu \neq 0$. We found that sometimes the function was not smooth enough to find the root easily, or roots were found to be close to a singularity complicating the numerical evaluation of the gradient of the function G , required during the Newton Raphson procedure. In some instances the function $G(z_1)$ had multiple roots, with only one of them describing the physical solution.

Instead of using the Newton-Raphson method to find a specific value for γ , we used the following method to find the original instability criteria given in Eq. (18): For each μ we looped through values of z_2 in the interval $[-10, 10]$, and for each z_2 we used Newton-Raphson to find the corresponding z_1 that satisfied the equivalent instability condition $p_1^2 q - \phi = 0$. We then found the values for γ and σ obtained for these values of z_1 and z_2 , and plotted σ as a function of γ for each μ . To plot Fig. 9 we used values of γ to be linearly spaced with intervals of 0.01. If the algorithm produced a value of γ within 0.001 of the required value, the corresponding σ_c was accepted as a suitable approximation. We found that for values of $\mu < -4$, an extremely small change in z_2 produced a large change in γ . This meant that the limits of machine precision caused insufficiently accurate values for γ to be produced.

-
- [1] Elton, C. S., *The ecology of invasions by animals and plants*, University of Chicago Press, Chicago, 2000.
 - [2] Macarthur, R., *Ecology* **36** (1955) 533.
 - [3] Gardner, M. R. and Ashby, W. R., *Nature* **228** (1970) 784.
 - [4] May, R. M., *Nature* **238** (1972) 413.
 - [5] May, R. M., *Stability and complexity in model ecosystems*, Princeton University Press, Princeton, NJ, 1973.
 - [6] Coyte, K. Z., Schluter, J., and Foster, K. R., *Science* **350** (2015) 663.

- [7] Foster, K. R., Schluter, J., Coyte, K. Z., and Rakoff-Nahoum, S., *Nature* **548** (2017) 43.
- [8] Allesina, S. and Pascual, M., *Theoretical Ecology* **1** (2008) 55.
- [9] Allesina, S. and Tang, S., *Nature* **483** (2012) 205.
- [10] Allesina, S. and Tang, S., *Population Ecology* **57** (2015) 63.
- [11] Tang, S., Pawar, S., and Allesina, S., *Ecology Letters* **17** (2014) 1094.
- [12] Grilli, J., Rogers, T., and Allesina, S., *Nature Communications* **7** (2016).
- [13] Gibbs, T., Grilli, J., Rogers, T., and Allesina, S., *Physical Review E* **98** (2018).
- [14] Mehta, M. L., *Random Matrices (Pure and applied mathematics, v. 142)*, Elsevier Science Limited, Amsterdam, 2004.
- [15] Berg, J. and Engel, A., *Physical Review Letters* **81** (1998) 4999.
- [16] Berg, J. and Weigt, M., *Europhysics Letters (EPL)* **48** (1999) 129.
- [17] Diederich, S. and Oppen, M., *Physical Review A* **39** (1989) 4333.
- [18] Biscari, P. and Parisi, G., *Journal of Physics A: Mathematical and General* **28** (1995) 4697.
- [19] Oliveira, V. M. D. and Fontanari, J. F., *Physical Review Letters* **85** (2000) 4984.
- [20] Mezard, M., Parisi, G., and Virasoro, M. A., *Spin glass theory and beyond*, World Scientific, Singapore, 1993.
- [21] Bunin, G., arXiv:1607.04734 (2016).
- [22] Bunin, G., *Phys. Rev. E* **95** (2017) 042414.
- [23] Biroli, G., Bunin, G., and Cammarota, C., *New Journal of Physics* **20** (2018) 083051.
- [24] De Dominicis, C., *Physical Review B* **18** (1978) 4913.
- [25] Martin, P. C., Siggia, E. D., and Rose, H. A., *Physical Review A* **8** (1973) 423.
- [26] Sommers, H. J., Crisanti, A., Sompolinsky, H., and Stein, Y., *Physical Review Letters* **60** (1988) 1895.
- [27] Coolen, A., Chapter 15 statistical mechanics of recurrent neural networks ii dynamics, in *Neuro-Informatics and Neural Modelling*, edited by Moss, F. and Gielen, S., volume 4 of *Handbook of Biological Physics*, pages 619 – 684, North-Holland, 2001.
- [28] Coolen, A. C. C., *The mathematical theory of minority games: statistical mechanics of interacting agents*, Oxford University Press, Oxford, 2005.
- [29] Hertz, J. A., Roudi, Y., and Sollich, P., *Journal of Physics A: Mathematical and Theoretical* **50** (2016) 033001.
- [30] Oppen, M. and Diederich, S., *Physical Review Letters* **69** (1992) 1616.
- [31] Galla, T., *Journal of Physics A: Mathematical and General* **39** (2006) 3853.
- [32] Galla, T., *Journal of Statistical Mechanics: Theory and Experiment* **2005** (2005).
- [33] Yoshino, Y., Galla, T., and Tokita, K., *Journal of Statistical Mechanics: Theory and Experiment* **2007** (2007).
- [34] Yoshino, Y., Galla, T., and Tokita, K., *Physical Review E* **78** (2008).
- [35] Galla, T., *Europhysics Letters (EPL)* **78** (2007) 20005.
- [36] Eissfeller, H. and Oppen, M., *Physical Review Letters* **68** (1992) 2094.
- [37] Roy, F., Biroli, G., Bunin, G., and Cammarota, C., *Journal of Physics A: Mathematical and Theoretical*

(2019).

- [38] Galla, T. and Farmer, J. D., Proceedings of the National Academy of Sciences **110** (2013) 1232.
- [39] Galla, T., EPL (Europhysics Letters) **123** (2018) 48004.
- [40] Sato, Y. and Crutchfield, J. P., Phys. Rev. E **67** (2003) 015206.
- [41] Holling, C. S., Memoirs of the Entomological Society of Canada **97** (1965) 5.
- [42] Hill, A. V., The Journal of Physiology **40** (1910) i.
- [43] Bunin, G., bioRxiv:484576 (2018).
- [44] Holling, C. S., The Canadian Entomologist **91** (1959) 293.
- [45] Holling, C. S., The Canadian Entomologist **91** (1959) 385.
- [46] Barbier, M. and Arnoldi, J.-F., bioRxiv:147728 (2017).
- [47] Simpson, E. H., Nature **163** (1949) 688.
- [48] Real, L. A., Ecology **60** (1979) 481.